INVITED PAPER

"Big Data Assimilation" Toward Post-Petascale Severe Weather Prediction: An Overview and Progress

This article summarizes the activities and progress of the big data assimilation project for severe weather prediction and concludes with perspectives toward the post-petascale supercomputing era.

By Takemasa Miyoshi, Guo-Yuan Lien, Shinsuke Satoh, Tomoo Ushio, Kotaro Bessho, Hirofumi Tomita, Seiya Nishizawa, Ryuji Yoshida, Sachiho A. Adachi, Jianwei Liao, Balazs Gerofi, Yutaka Ishikawa, Masaru Kunii, Juan Ruiz, Yasumitsu Maejima, Shigenori Otsuka, Michiko Otsuka, Kozo Okamoto, and Hiromu Seko

ABSTRACT | Following the invention of the telegraph, electronic computer, and remote sensing, "big data" is bringing another revolution to weather prediction. As sensor and computer technologies advance, orders of magnitude bigger data are produced by new sensors and high-precision computer simulation or "big simulation." Data assimilation (DA) is a key to numerical weather prediction (NWP) by integrating the real-world sensor data into simulation. However, the current DA and NWP systems are not designed to handle the "big data" from next-generation sensors and big simulation. Therefore, we propose "big data assimilation" (BDA) innovation to fully utilize the big data. Since October 2013, the Japan's BDA project has been exploring revolutionary NWP at 100-m mesh refreshed every 30 s, orders of magnitude finer and faster than the current typical NWP systems, by taking advantage of the fortunate combination of next-generation technologies: the 10-petaflops K computer, phased array weather radar, and geostationary satellite Himawari-8. So far, a BDA prototype system was developed and tested with real-world retrospective local rainstorm cases. This paper summarizes the activities and progress of the BDA project, and concludes with perspectives toward the post-petascale supercomputing era.

KEYWORDS | Atmospheric measurements; computer applications; Kalman filtering; optimal control; phased array radar; remote sensing; simulation; supercomputers; weather forecasting

Manuscript received January 15, 2016; revised April 5, 2016 and August 7, 2016; accepted August 15, 2016. Date of publication September 26, 2016; date of current version October 18, 2016. This study was supported by CREST, Japan Science and Technology Agency (JST). *(Corresponding author: Takemasa Miyoshi.)*

T. Miyoshi is with the RIKEN Advanced Institute for Computational Science, Chuo-ku, Kobe 650-0047, Japan, with the Department of Atmospheric and Oceanic Science, University of Maryland, College Park, MD 20740 USA, and also with the Application Laboratory, Japan Agency for Marine-Earth Science and Technology, Yokohama 236-0001, Japan (e-mail: takemasa.miyoshi@riken.jp).

G.-Y. Lien, **H. Tomita**, **S. Nishizawa**, **R. Yoshida**, **S. A. Adachi**, **B. Gerofi**, **Y. Ishikawa**, **Y. Maejima**, and **S. Otsuka** are with the RIKEN Advanced Institute for Computational Science, Chuo-ku, Kobe 650-0047, Japan (e-mail: guo-yuan.lien@riken.jp; htomita@riken.jp; s-nishizawa@riken.jp; ryoshida@riken.jp; sachiho.adachi@riken.jp; bgerofi@riken.jp; yutaka.ishikawa@riken.jp; yasumitsu.maejima@riken.jp; shigenori.otsuka@riken.jp).

S. Satoh is with National Institute of Information and Communications Technology, Koganei 184-8795, Japan (e-mail: satoh@nict.go.jp).

T. Ushio is with the Osaka University, Suita 565-0871, Japan (e-mail: ushio@comm.eng.osaka-u.ac.jp).

K. Bessho was with the Meteorological Satellite Center, Kiyose 204-0012, Japan. He is now with the Forecast Department, Japan Meteorological Agency, Tokyo 100-8122, Japan (e-mail: kbessho@met.kishou.go.jp).

J. Liao was with the RIKEN Advanced Institute for Computational Science, Chuo-ku, Kobe 650-0047, Japan. He is now with the Southwest University of China, Chongqing 400715, China (e-mail: jianwei.liao@riken.jp).

M. Kunii, **M. Otsuka**, and **K. Okamoto** are with the RIKEN Advanced Institute for Computational Science, Chuo-ku, Kobe 650-0047, Japan, and also with the Meteorological Research Institute, Tsukuba 305-0052, Japan (e-mail: mkunii@mri-jma.go.jp; motsuka@mri-jma.go.jp; kokamoto@mri-jma.go.jp).

J. Ruiz is with the RIKEN Advanced Institute for Computational Science, Chuo-ku, Kobe 650-0047, Japan, and also with the CIMA, CONICET-University of Buenos Aires, Buenos Aires, Argentina (e-mail: jruiz@cima.fcen.uba.ar).

H. Seko is with the Meteorological Research Institute, Tsukuba, Japan (e-mail: hseko@mri-jma.go.jp).

Digital Object Identifier: 10.1109/JPROC.2016.2602560

I. INTRODUCTION

Weather prediction has been revolutionized due to new technological developments such as the invention of the telegraph, electronic computer, and remote sensing. The telegraph enabled plotting weather charts in the mid-19th century once we could exchange weather observation data for a long distance quickly. About 100 years later, Charney *et al.* (1950) pioneered to run a computer simulation of the weather successfully using the first general-purpose electronic computer ENIAC. In 1955, the U.S. Joint Numerical Weather Prediction Unit started operational numerical weather prediction (NWP) using one of the earliest mainframe machines IBM 701. Since then, the computer has been growing rapidly, and NWP with high-performance computers (HPCs) became a key technology for weather prediction. In the 1970s, space exploration technologies enabled satellite remote sensing. A number of weather satellites have been launched, and it was essential to incorporate as soon as possible these new data into NWP. The present weather prediction largely relies on NWP with HPCs and satellite data. The method of integrating computer simulations and real-world data is known as data assimilation (DA), which plays an equally important role in NWP as the time-evolving simulation model.

Now "big data" are bringing another revolution to weather prediction. Here we focus on so-called "science big data" coming from advanced sensors and computer simulation, distinguished from broad-sense "big data" including social media and business data. New sensors produce orders of magnitude more data than the current sensors, and capture detailed structures of rapidly changing, small-scale weather. We can run simulations of these small-scale weather by utilizing highest end supercomputers and performing high-resolution "big simulations." These big data from new sensors and "big simulations" will revolutionize NWP. However, the existing NWP and DA systems are not designed to process such rapid and dense observations, therefore, we need to bring innovation to DA and NWP, i.e., what we call "big data assimilation" (BDA) innovation [23]. BDA will enable orders of magnitude more precise and rapidly updated weather prediction, providing an early warning to pinpoint local sudden severe events such as tornadoes, torrential rain, flooding, landslides and lightning strikes, threats to life and property.

Much effort has been devoted to explore convective-scale DA and NWP so far. The U.S. effort on "Warn-on-Forecast" project [39], [40] aims to extend the forecasting capability of severe weather using convective-scale DA and NWP instead of the traditional observation-based approach. Sun *et al.* [41] provided a comprehensive review on the state of the art of using NWP for nowcasting convective precipitation. The goal of BDA shares the ones of these previous and ongoing efforts, but extends toward 10 or 20 years in the future by taking advantage of the fortunate combination of Japan's most advanced developments on next-generation supercomputing and sensing technologies: the 10-petaflops "K" supercomputer, the phased array weather radar (PAWR [42], [44]), and the geostationary meteorological satellite Himawari-8 [1]. BDA extends the previous efforts and explores what we could do to address the challenge for convective-scale DA and NWP by fully utilizing "big data" from the future-generation supercomputing and sensing technologies.

Miyoshi *et al.* [23] presented a short report to the meteorological community on the concept of BDA and the first proof-of-concept experimental results. In this paper, we present the entire view of the broader BDA activities including the most recent progress and future perspectives toward post-petascale HPC. We aim to make this paper a single point of reference about the Japan's BDA project started in October 2013 as a frontier activity of big data in use and applications for convective-scale DA and NWP.

In Section II, we will describe an overview of the BDA system, followed by Sections III–V describing the details on the components of the BDA system. Section III summarizes the big data from advanced observations, PAWR, and geostationary satellite Himawari-8. Section IV describes the other component involving big data, big simulation. Section V describes the challenge on big data handling in an HPC. Then, the experimental results on a couple of real-world retrospective local rainstorm cases are presented in Section VI, although Himawari-8 data were not used yet. Section VII describes the potential use of Himawari-8. Finally, Section VIII provides conclusion and future perspective.

II. BIG DATA ASSIMILATION: AN OVERVIEW

The Japan's BDA project started in October 2013 as one of the first two projects funded by the Japan Science and Technology Agency (JST) government strategic basic research program "CREST" in the research area "Advanced Application Technologies to Boost Big Data Utilization for Multiple-Field Scientific Discovery and Social Problem Solving" (research supervisor: Prof. Y. Tanaka).

We first describe the general workflow of the BDA system (Fig. 1), and later discuss what is different or revolutionary from the current DA and NWP systems. The details of each component are described in the following sections, so that this section focuses on providing a bird's eye view on the whole BDA system. Fig. 1 shows the general workflow of the BDA system. PAWR is capable of observing dense 3-D reflectivity (reflecting signals mainly from precipitating clouds) every 30 s, and Himawari-8 can observe visible and infrared radiances every 2.5 min or even 30 s in a limited area (cf., Section III). The BDA system is designed to fully take advantage of the observation big data in the real time. At time 0, we start to receive the observations for the previous 30 s (time −30 to 0)

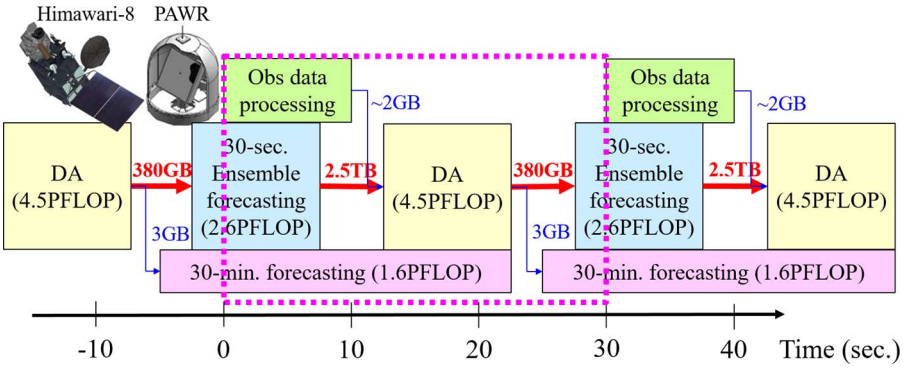

Fig. 1. ***General workflow of the BDA system. Shown at the top left corner are Himawari-8 and PAWR, providing new observation data every 30 s. The magenta dotted box indicates a 30-s time window from time 0 to 30. The computational amount for 30-s ensemble forecasting and DA is shown in the unit of 10^{15} floating point operations (PFLOPs) as obtained by Miyoshi et al. [23].***

from the observation sites; at time 30, we start to receive the next set of data. Therefore, the data at time 0 need to be processed in 30 s, otherwise, the data come faster than the processing speed, and the system does not work in real time. The data are processed quickly (green box), and transferred to an HPC, in the present case, the K computer. The yellow DA box takes the observation data and 30-s forecast data, and outputs the best estimate of the atmospheric state. This best estimate is then used as the initial condition for the next forecast. The 30-min forecast (magenta box) using the observation data up to time 0 will be available at about time 60, or 1 min later than the observation end time. Namely, we have a 29-min forecast lead time effectively.

Data assimilation (DA) is a widely studied method in NWP and other geophysical applications to optimally combine the observations and simulation, and makes the simulation best represent the real world [11]. For weather forecasting, it is known that DA plays an equally important role as the simulation model in NWP. Fig. 2 indicates the general framework of NWP. The blue curve indicates unknown true atmospheric evolution, and we simulate the atmospheric evolution initialized by the best estimate of the current state, also known as the analysis (purple boxes). Due to the chaotic nature of the atmospheric dynamics, the initial error is expected to grow. Therefore, the short-term forecasts (blue boxes) are expected to have larger errors than the analyses, and the

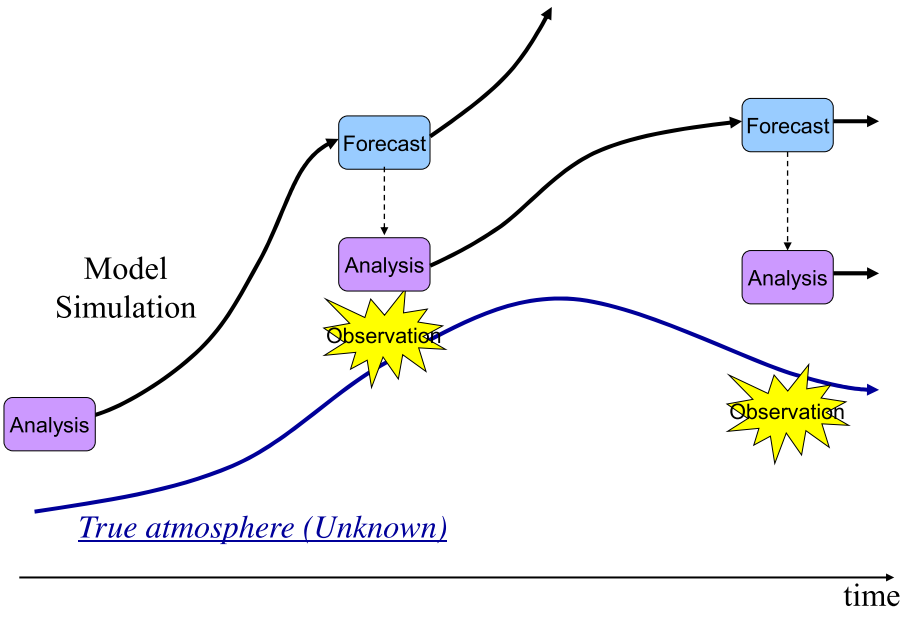

Fig. 2. ***Schematic of numerical weather prediction.***

forecast error keeps growing if we run a longer simulation. Once we obtain observation data (yellow stars), the DA algorithm combines the short-term forecast and observation data and produces the analysis. This way, we make the simulation keep the track of the true atmosphere, enabling NWP.

The DA algorithm is based on the optimal control, statistical mathematics and dynamical systems theory. We consider the error statistics of the forecast and observation data, and find the optimal combination. To represent the error statistics, if we assume the simple normal distribution, the mean and covariance are required. Let N be the system dimension, typically $N = \mathrm{O}(10^7)$ or larger in NWP, and the mean and covariance have the dimensions of N and N^2, respectively. The basic idea is the same as the control theory, but the difference lies in the large dimensionality, which has been a big challenge in atmospheric DA. Recently, an ensemble-based approach was common, representing the error by a limited number of samples, say, m samples. This requires running m parallel simulations, so that the sample size is usually limited to about 100 or less, i.e., $m \ll N$. Miyoshi *et al.* [21], [22] explored an extreme of a large sample size $m = 10240$, but still this is only a percent of $N = \mathrm{O}(10^7)$. Efficient algorithms to use the small sample size m have been explored extensively, and the local ensemble transform Kalman filter (LETKF [8]) is a widely used method. The LETKF has been applied to various geophysical systems including operational global and regional NWP models [19], [20], and the BDA system employs the LETKF.

Radar DA using a similar method has been widely studied in the meteorology community (e.g., [38], [45], and [46]), and what is new and revolutionary in the BDA system is the extreme size of the problem. Table 1 summarizes the problem sizes for the BDA, operational, and research systems. Here we show typical state-of-the-art operational systems, the Japan Meteorological Agency (JMA) Local Forecast Model (LFM [6]) and the U.S. National Oceanographic and Atmospheric Administration (NOAA) High-Resolution Rapid Refresh (HRRR, http://ruc.noaa.gov/hrrr), and typical research systems. The resolution of BDA is about ten times more than the operational and research systems. Ten times more resolution requires roughly 10 000 times more computations for a simulation for a unit time if we consider four dimensions in space time. Another big difference is the update frequency. BDA is 120 times faster than hourly updated systems. Namely, BDA requires the processing of 10 000 times more computations in a 120th of time. If we can achieve this extremely challenging throughput and fully exploit the big data, BDA will bring a revolution to severe weather prediction by providing pinpoint 100-m mesh simulation of each individual convective cell for the next 30 min. This is essential if we consider the rapid development of the local severe weather events such as tornadoes and torrential rains. Warnings in even only 10-min lead time could save lives from this devastating weather.

To achieve the extreme throughput, we need to bring innovations to accelerate the following:

1) observation data processing and transfer (Section III);
2) simulation (Section IV);
3) DA;
4) data transfer between simulation and DA (Section V).

As shown in Fig. 1, we have a strict time limit to finish these computations. Sections III–V discuss each component except for DA, and Section VI shows the results for two real-world retrospective torrential rain cases. The algorithmic details of the LETKF itself, in particular, including the parallel efficiency, are provided by Hunt *et al.* [8] in a comprehensive manner, and we will not repeat them in this paper.

III. BIG DATA FROM ADVANCED OBSERVATIONS

A. PAWR for Use in BDA

Recent progress of information and communication technologies enabled a rapid scanning radar system. In

Table 1 Comparison of the Problem Size of Convective-Scale DA and NWP for BDA, Operational, and Research Systems

	Resolution	Update frequency	Forecast duration
BDA	100 m	30 seconds	30 minutes
JMA LFM (operational)	2 km	1 hour	9 hours
NOAA HRRR (operational)	3 km	1 hour	15 hours
Yussouf et al. (2013)	2 km	3 minutes	1 hour
Chang et al. (2014)	1 km	5 minutes	1.5 hours
Jones et al. (2015)	3 km	5 minutes	1.5 hours

2012, Toshiba Corporation and Osaka University developed a new type of the PAWR system [42], [44] under a contract with the Japanese National Institute of Communication and Information Technology (NICT) and installed the first PAWR system in Suita Campus, Osaka University (Fig. 3). The PAWR has a 1-D phased-array antenna at X-band (9 GHz), operated with an electronic scan in the elevation direction and a mechanical rotation in the azimuth direction. To reduce the time for the 3-D volume scan, we use a fan-beam transmission and a digital beam forming (DBF) reception using 128 antenna elements. The PAWR can scan the whole sky within 30 s up to 60 km in radius over 100 elevation angles, and the corresponding data volume reaches about 100 times of the one from a typical parabolic-antenna radar which observes the whole sky within 5–10 min for about 15 elevation angles. The initial observation results demonstrate the unique capability of the new PAWR system. In this section, the basic principle of the new PAWR technology and observation results are described.

1) Phased Array Weather Radar: Until now, the parabolic-antenna radar system has been widely used all over the world to observe precipitation near the surface. The conventional radar system such as the U.S. National Weather Service's NEXRAD and JMA's national radar network usually uses the S- or C-band frequency, and a single radar can cover wide area over a few hundreds of kilometers. However, the small-scale meteorological phenomena such as tornado outbreaks and torrential rain events may be missed because the temporal and spatial resolution of the parabolic-antenna radar network is several minutes and a few hundred meters, almost equal or worse than the rapid and small-scale phenomena. To fully capture such small-scale severe weather phenomena, a fast scanning and higher resolution radar system is required.

So far, several kinds of fast scanning radar systems have been developed mainly for research use. Krehbiel and Brook [14] developed a unique radar system called "Red Ball RADAR" using a broadband noise signal, and after that, Doppler on wheels (DOW; [43]) and mobile phased array radar (MWR-05XP; [2]) were developed with hybrid approaches. More recently, atmospheric imaging radar (AIR) was developed [9] with a similar approach to the PAWR in this study.

The PAWR at the X-band in this project takes an electronic scanning for elevation observation and mechanical scanning for azimuth observation to achieve the 100-m resolution for 100 elevation angles every 30 s (i.e., rotation speed of two rounds per minute) up to 60 km in radius, or every 10 s (six rounds per minute) up to 30 km in radius. The system transmits a broad fan-beam of 5°–15° with 24 antenna elements and the backscattered signals are received with 128 antenna elements. The signal processor at the back of the antenna elements sharpens the received beam every 1°. This process is repeated a few times up to 90° in elevation (i.e., the zenith angle). The time for the electronic scanning for elevation is within 80 ms. By rotating the antenna in azimuth, the full 3-D volume scan with 30-s and 100-m resolution is achieved.

2) A Case on July 13, 2013: The PAWR system was installed at the top of the Electrical Engineering Department building at Osaka University in June 2012 (Fig. 3) and the routine observation started just after the installation. Fig. 4 shows an example of the precipitation system

Fig. 3. ***Photographs of the PAWR at Suita Campus, Osaka University (cf., [42, Fig. 10]). (Left) PAWR at the top of the Electrical Engineering Department building at Osaka University. (Right) Antenna of the PWAR system inside the Radar Dome.***

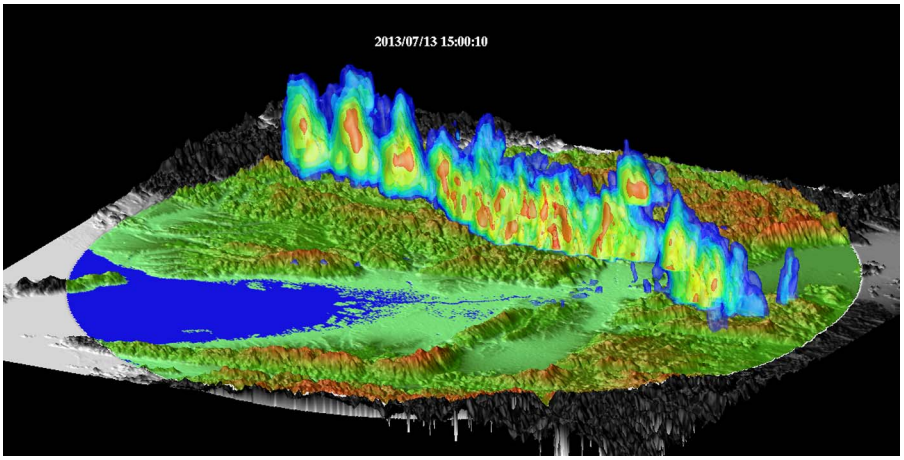

Fig. 4. ***Reflectivity observed by the PAWR on July 13, 2013.***

observed by the PAWR. This band-type precipitation system was observed on July 13, 2013 and produced heavy precipitation in Kyoto and Osaka. The precipitation system consists of more than ten thunderstorm cells, and in each cell the precipitation cores with large reflectivity appear at 2–5-km height. With the very high spatial and temporal resolution of the PAWR system, we can find that the developing precipitation cores are moving downward (Fig. 5), demonstrating a great advantage of the PAWR. This downward motion is not usually captured by conventional parabolic-antenna radars. Meanwhile, the dense vertical resolution of 100 elevation angles captures the detailed vertical structure of the thunderstorm cells; this is also impossible for the conventional radar system with ten or so elevation observations with timing delays. These observation results show a unique potential capability of the new PAWR system. The impressive 30-s and 100-m resolution data over 100 elevation angles can reveal the detailed structure of thunderstorm dynamics, and they will be useful for the early and precise detection of torrential rain systems.

3) Processing of Big Data From PAWR: The normal data rate of the PAWR is 131 Mb/s, approximately 100 times bigger than a typical traditional parabolic-antenna radar. The size of a single volume scan of the PAWR is ten times bigger than that of a traditional radar using parabolic antenna. In typical traditional radar with the range resolution of 150 m, the volume scan is composed of 15 elevation angles in 5 min. Since the time of 30 s

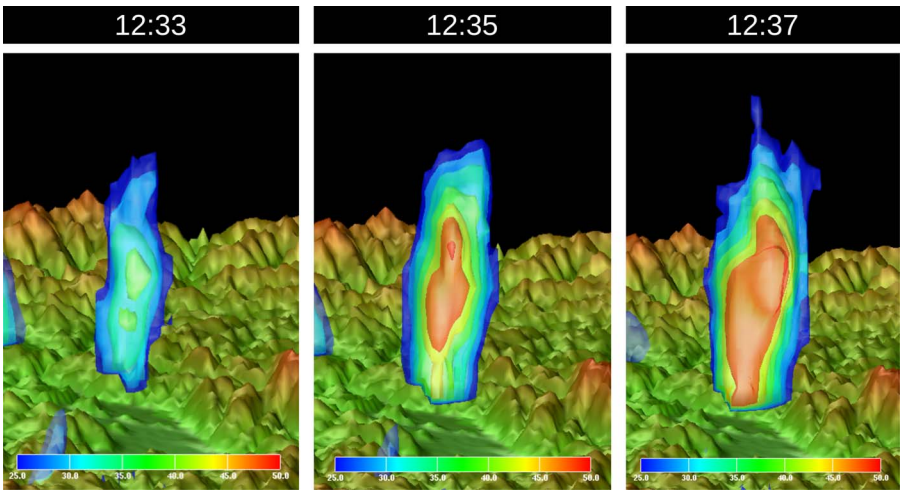

Fig. 5. ***Time series of reflectivity for a thunderstorm core observed by the PAWR on July 13, 2013. The every-2-min images show the downward motion of the developing precipitation core, which is hardly captured by the conventional radar system.***

for a PAWR volume scan is ten times faster than the traditional radar, the total data rate is 100 times bigger than the traditional radar.

Big data from PAWR should be processed in real time for the BDA system. We developed a fast data processing and transfer system as shown in Fig. 6. The radar site in Osaka is connected to the data processing, archiving and publishing site in Tokyo using a fast network (JGN-X) of 10 Gb/s. The system is built out in the NICT science cloud [24], providing facilities for data processing and publishing. This data system can transfer the maximum original data of 220 Mb/s from the radar site to an archive storage in real time without delay. Therefore, the challenge to the real-time system lies in the data processing procedure including data quality control (QC). It is simple to make a quick-look rainfall map for publishing in a web-page within one minute after the radar observation finishes (http://pawr.nict.go.jp/index_en.html). However, in the case of BDA, the data quality is important, and the processing time for QC is a challenge.

4) Quality Control: The original data of PAWR include many useless data for BDA. For example, even if there is no rain, reflectivity is observed due to ground clutter echoes or abnormal noise data by various reasons such as echoes from flying insects. We have to reject such nonmeteorological echoes and abnormal data. Also, it is important to distinguish missing data from no precipitation. Zero precipitation is useful for DA, but missing data provide no information. For example, Fig. 7 shows reflectivity in a clear day, and Doppler velocity map in a broad area of stratiform rainfall. These figures show typical ground clutter echoes, blocking area, and noise signals.

Ruiz *et al.* [33] developed a QC algorithm for the BDA experiments. The QC algorithm considers four parameters: texture of reflectivity (Ze) patterns, radial velocity, Ze correlation with time, and Ze vertical gradient. To reject clutter echoes completely, a Bayesian classification algorithm was adopted. The QC algorithm is very effective in removing the bad-quality data, but it requires processing time much longer than 30 s at this moment. For the real-time BDA system, developing a faster QC algorithm is a challenge, and we are now working on the development.

B. Himawari-8 for Use in BDA

Japan's new geostationary meteorological satellite Himawari-8 was successfully launched from Tanegashima Space Center, Japan, using an H-IIA rocket on October 7, 2014 [1]. JMA has started its operations from July 7, 2015 as a successor of Multi-functional Transport SATellite (MTSAT)-2. Advanced Himawari Imager (AHI) onboard Himawari-8 has a rich observation functionality compared with MTSAT-2/Imager. AHI has 16 observation bands, compared with five bands of the previous MTSAT-2/Imager. The spatial resolutions of AHI visible and infrared bands are twice as high as those of MTSAT-2/Imager. As for the observation frequency, MTSAT-2/Imager scans the entire visible hemisphere (also known as full disk) every hour and the visible part of the northern hemisphere every half hour. Alternatively, Himawari-8/AHI scans the full disk every 10 min, and simultaneously scans limited domains such as the Japan area and an arbitrarily chosen targeting area every 2.5 min. These enhancements lead to about 50 times more data obtained by AHI than the previous generation imagers.

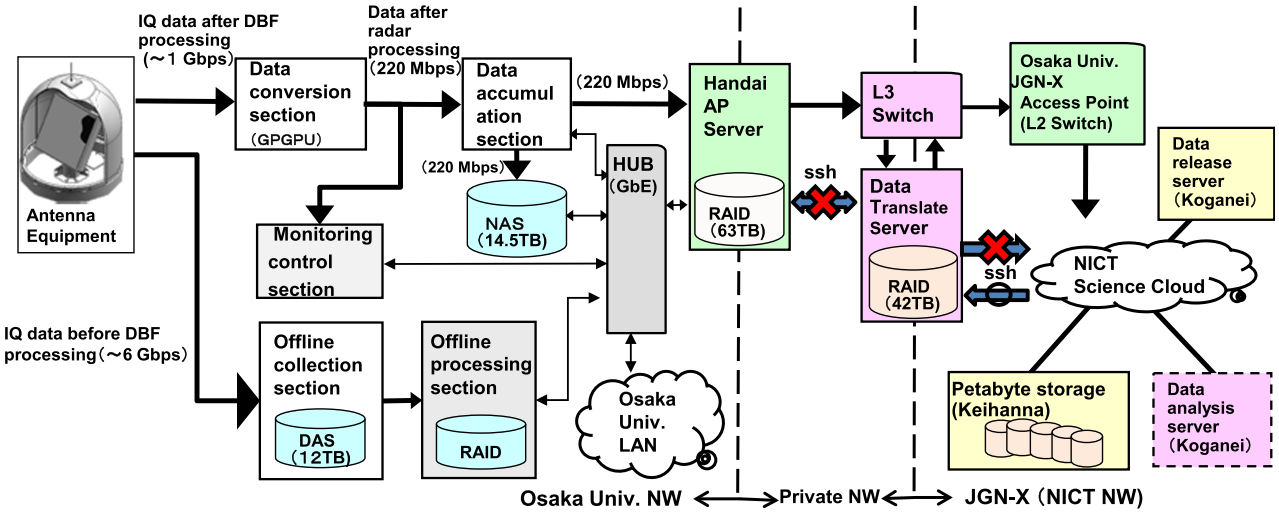

Fig. 6. *The real-time data processing and transfer system (adopted from Fig. 7 of NICT News January 2013 issue, http://www.nict.go.jp/en/pdf/NICT_NEWS_1301_E.pdf).*

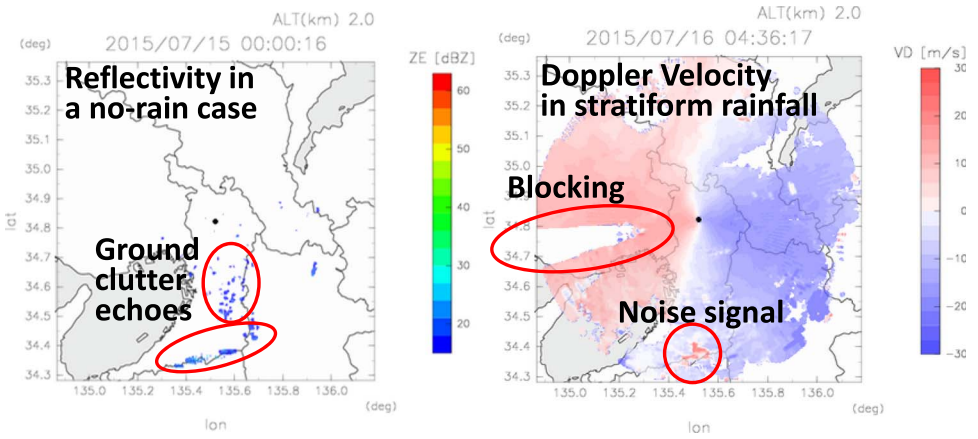

Fig. 7. ***Examples of candidates of data quality control.***

The BDA project will explore the potential advantage of assimilating Himawari-8/AHI observation data for improving severe weather forecasts. To assimilate the AHI observation data with high-resolution NWP, high-precision image navigation and calibration are essential. The image navigation of AHI is as precise as 1 km, and the accuracy of band-to-band coregistration is in the same range. These are validated based on a landmark analysis using a pattern matching approach. The infrared band calibration is as accurate as 0.2 K without significant diurnal variations, and has been validated using an approach developed under an international calibration framework of Global Space-based Inter-Calibration System (GSICS) [4]. The calibration performance for visible and near-infrared bands (total six bands) is investigated through comparisons with other earth observing satellites and a radiative transfer model, showing that two bands (1.6 and 2.3 μm) may have potential biases by around 5% and that the other four bands (0.47, 0.51, 0.64, and 0.86 μm) have no significant bias. To improve validation reliability, other approaches such as a lunar irradiance model [12] are in preparation. Monitoring the difference between the current and previous images is also an effective tool to check AHI data quality on a near-real-time basis. More details on the validation results are described by Okuyama *et al.* [28].

With the dramatic enhancement of observing capability by Himawari-8, the physical products derived from the satellite imager are significantly enhanced. First, the product of atmospheric motion vectors (AMVs) are improved by taking advantage of Himawari-8's high spatial and temporal resolution. AMVs are satellite-derived wind products by analyzing cloud motion and height from a satellite imagery animation. They are used in the operational global NWP systems, and provide precious information about the atmospheric flow, especially over the ocean and data-scarce regions. The Meteorological Satellite Center (MSC) of JMA has developed an enhanced algorithm for effective use of high spatial, temporal, and spectral resolution of Himawari-8/AHI. The motion tracking is enhanced by extracting large-scale cloud features and using the cloud motion before the analysis time as prior information. This brings substantial improvement on small-scale cloud motion vectors and significantly decreases the errors of AMVs. As for the height assignment, an optimal estimation method was developed to minimize the difference between the observed and theoretical radiance values for three or more bands. This new algorithm improved the spatial coverage and the number of quality controlled AMVs. Due to the enhanced capability of Himawari-8 and the new algorithm, Fig. 8 shows a significantly larger number of AMVs derived from Himawari-8 compared with those from the previous-generation MTSAT-2.

MSC has also developed an algorithm for the fundamental cloud product, which is used for several other physical products from Himawari-8, and continues to improve the accuracy. The algorithm is based on the method developed by the European Organization for the Exploitation of Meteorological Satellites (EUMETSAT)/Nowcasting Satellite Application Facility (NWC-SAF) [18] and the National Oceanic and Atmospheric Administration (NOAA)/National Environmental Satellite, Data, and Information Service (NESDIS) [31]. The fundamental cloud product consists of cloud mask (presence or absence of cloud), cloud type (opaque/semitransparent/fractional), could phase (ice/water/mixed), and cloud top height at 100-m resolution (cf., Fig. 9). Each element is calculated with the threshold that is set by comparing the observation value with the result of radiation calculation statistically [1]. The spatial resolution is one pixel of the infrared bands (2 km at the subsatellite point). The fundamental cloud product has not been used in DA and NWP so far, but may be useful. For example, capturing a rapid change of cloud top height every 2.5 min may help improve DA and NWP for a rapid convective development.

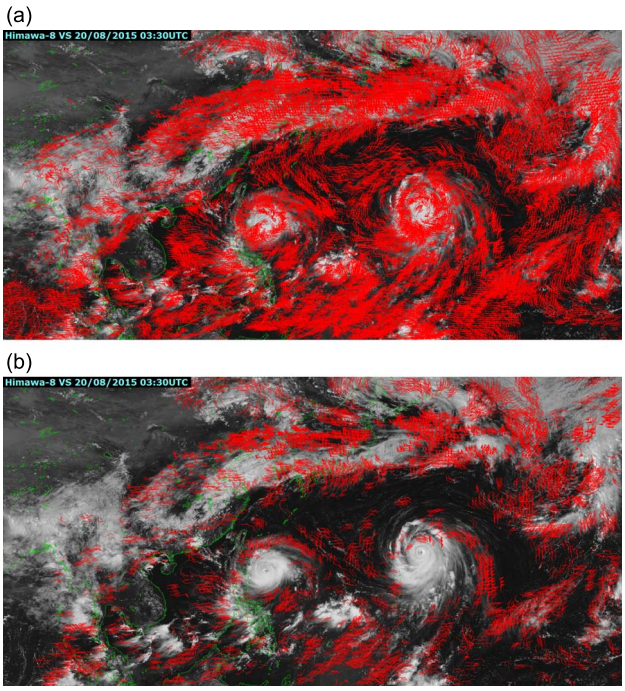

Fig. 8. *(a) Himawari-8 visible image (greyscale) and spatial distribution of AMVs (red barbs) at 0300 UTC, August 20, 2015 derived from Himawari-8 infrared (10.4 μm) and visible (0.64 μm) images with the new algorithm. Green lines indicate coastlines. (b) Similar to (a), but for AMVs from MTSAT-2 infrared and visible images.*

IV. BIG SIMULATION

Taking advantage of Japan's flagship 10-petaflops K computer, the BDA system includes 100-m mesh "big simulation" to resolve individual convection. Previous studies on convective-scale DA and NWP have been using O (1 km)-mesh simulations (Table 1), and the 100-m mesh is an order of magnitude smaller. If we consider the two dimensions in the horizontal, and vertically and temporally higher resolution as well, then the required computations are increased by a factor of 10 000. Moreover, the BDA system requires 100 ensemble simulations. In this section, we describe the requirements of the simulation model for the real-time BDA system. To effectively utilize high-resolution observational data from PAWR and Himawari-8, the simulation should be highly sophisticated in terms of the following viewpoints.

1) Large domain at high resolution. Cloud resolving models (CRMs) with the horizontal resolution at O(1 km) can capture the essential mechanism of deep convection typically at the horizontal scale of several kilometers. However, the O(1 km)-mesh model is still too coarse to resolve the detailed structure of deep convection. Drastically higher resolution at O(100 m) and a larger number of vertical levels bring a qualitative change; we can apply a large eddy simulation (LES) based on more reliable principles in the dynamical core. In addition, the domain size should be larger for capturing organized phenomena such as a convective complex while resolving each individual deep convection. A domain size of O((100 km)^2), i.e., about 1000 by 1000 grid points, will be necessary.
2) Sophisticated modeling on atmospheric physical processes. The performance of the model simulation depends on not only the resolution but also the degree of sophistication of model physics. For our BDA study, the two most important physical processes are turbulence and cloud microphysics. Atmospheric radiation is also important particularly for climate simulations, but we would expect that the impact of radiation for a very short time less than an hour would be limited. As for the turbulence process, the LES technique can be applied at 100-m resolution. With the LES, not only the planetary boundary layer processes but also mixing processes at the cloud boundaries are more explicitly simulated. As for the cloud microphysics, which has a direct impact on the representation of clouds, more complicated algorithms such as the multimoment bulk and spectral bin methods are

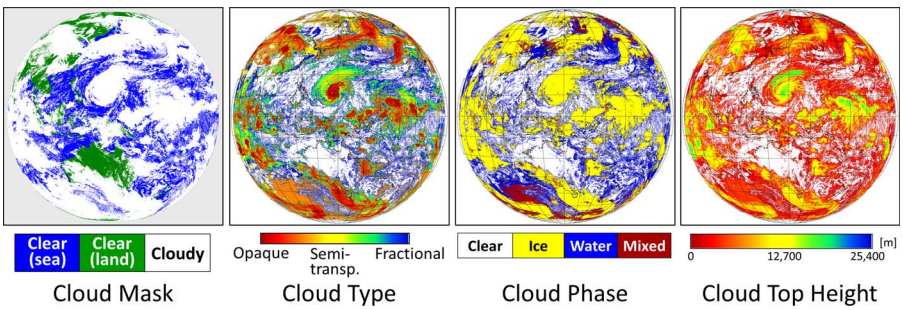

Fig. 9. *Fundamental cloud product at 0200 UTC April 10, 2015.*

promising. However, their computational costs are much higher than a simpler one-moment bulk method. When we choose the cloud microphysics schemes, the computational cost and physical complexity are the tradeoffs. The one-moment bulk method is widely used in cloud-resolving NWP mainly because of the low computational cost. It would also be a good choice for replicating the mechanisms of convective clouds, their organization, and lifecycle evolution. Since BDA poses strict time constraints, we choose the computationally cheaper one-moment bulk model for the prototype BDA system, and tune it well for the targeted region. The application of more sophisticated microphysics models is an important research subject for further improvements.

Table 2 summarizes the current target resolution and timing with the model configuration for BDA. The 100-m resolution is chosen in consideration of the resolution of PAWR and the capability of the K computer. Miyoshi *et al.* [23] measured the computational amount from the target configuration as shown in the boxes of Fig. 1 (cf., [23, Table 1]), and discussed that 5% of the 10-petaflops peak performance of the K computer will be able to run this system in real time. The target timing is essential for real-time application as new data keep coming every 30 s (Fig. 1). To make the BDA cycle feasible, the model simulation in a DA cycle needs to be finished within 10 s. For the 30-min forecast run, the timing requirement is not as strict, but this timing determines when the forecast is available. To prepare for the fast-growing convective weather risks, faster is better. We set this timing requirement as 30 s, which makes it possible to issue the forecast within 1 min after the observation (Fig. 1). This is very challenging from the computational aspect; the 100 ensemble simulations require a large capacity of a computer system, and the very short elapsed time for simulations requires a strong scalability. The BDA demands a high level of modeling techniques that can effectively utilize a large computer resource.

A. The SCALE-LES Model

To meet the requirement, we have developed a high-performance model named SCALE-LES [25], [37] suitable to the K computer. The SCALE-LES is based on the Scalable Computing for Advanced Library and Environment (SCALE; http://scale.aics.riken.jp/), a basic library and environment for meteorological numerical simulation models suitable to massively parallel HPC.

So far, SCALE-LES has produced promising results for cloud dynamics with idealized experiments at resolution up to 35 m, much higher than typical NWP research (e.g., [35] and [36]). The model also performs well for real cases. Fig. 10 shows an example of a real-world typhoon simulation in Japan. Using a three-domain multiple nesting approach, the simulation is downscaled from the global model (the JMA operational Global Spectral Model) to the target area in our BDA project. The horizontal spatial resolutions of the three nested domains are 7.5, 2.5, and 0.5 km, respectively. Here, the nesting is one way, so that the inner domains' boundary conditions come from the immediate outer domains, without feedback from the inner to the outer domains. An advantage of using SCALE-LES is an enhanced nesting system design. Different from the conventional nesting systems, the computations of the inner-most model are run in parallel to the outer models by splitting the MPI processes, and the computational efficiency is improved by 20%–30% in the case of Fig. 10 (Yoshida *et al.*, 2016, submitted to *Parallel Computing*).

B. Computational Performance and Scalability

To investigate the scaling performance of SCALE-LES on the K computer, we performed a series of experiments using different problem sizes (Table 3). Here, the number of horizontal grid points in a computational

Table 2 BDA Target Model Configuration and Timing Requirement

Domain size	100km x 100km x 20km(vertical)	
Resolution	100m mesh in the horizontal , 100 layers in the vertical	
Model physics	Turbulence : Large Eddy Simulation Microphysics: Well-tuned one-moment bulk method Other components: Radiation, land surface are almost same as the conventional cloud resolving model	
	Data assimilation cycle	Prediction run
Integration time	30sec	30min
Ensemble number	100	1
Elapse time	within 10 seconds	within 30 seconds

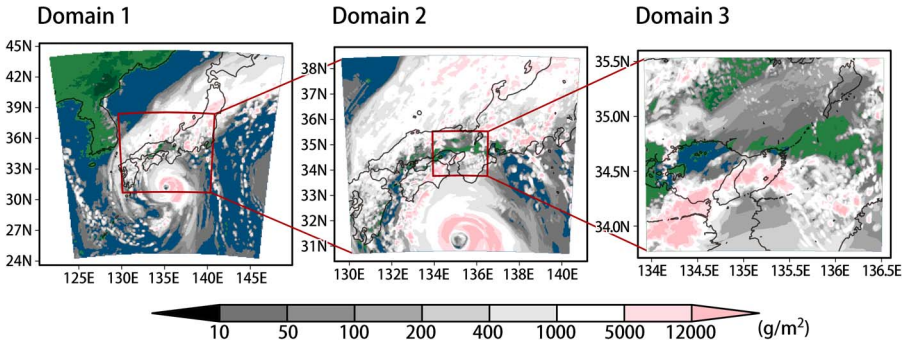

Fig. 10. *A snapshot of a real-case atmospheric simulation by SCALE-LES at 0200 UTC, September 21, 2011. The color shades show the vertically integrated hydrometeor quantities (g m^2).*

node varies from 8000 to 64 grid points. This type of experiments is known as the strong scaling experiments, by which we can find how much acceleration is achieved by using more parallel computational nodes. To match the actual target problem of BDA, the horizontal grid spacing is set to be 100 m with 100 vertical levels, and the integration time is 30 s. The communication time is measured using 12 computational nodes. The time steps of dynamics, microphysics, turbulence, and radiation are chosen to be 0.1, 10, 0.4, and 30 s, respectively. All floating-point computations are performed with "double-precision" variables by default in the SCALE model.

Fig. 11(a) shows the results of the strong scaling experiments for SCALE-LES. The most time-consuming part is the dynamics, and its scaling factor tends to be saturated by decreasing the problem size. This degradation of scaling comes from the load imbalance between eight threads: in the dynamics, the number of the outermost loop is not a multiple of 8. Furthermore, as shown in Fig. 11(b), the increasing ratio of the communication time among computational nodes with the decreasing problem size also leads to the saturation. On the other hand, the scaling of physics gives relatively ideal scaling. In addition, the I/O part is not a bottleneck. Table 3 also shows the elapsed times for each run (the sixth row).

C. Use of Single-Precision Variables for BDA

From the criterion that the simulation in a DA cycle should be finished within 10 s, the horizontal grid number should be smaller than N512, which requires 180000 nodes for 100 ensemble simulations (Table 3). This exceeds the capacity of the K computer with less than 90000 nodes. We could reduce the problem size such as

Table 3 List of the Strong Scaling Experiments. The Domain Size Is Chosen to be 100-km-by-96-km for N8000, N4000, and N2000, and 96-km-by-96-km for Other Experiments

Experiments	N8000	N4000	N2000	N1280	N512	N256	N128	N64
# of grid points in 1 node (imax x jmax)	100x80 (=8000)	50x80 (=4000)	50x40 (=2000)	32x40 (=1280)	32x16 (=512)	16x16 (=256)	16x8 (=128)	8x8 (=64)
Domain size in 1 node (km x km)	10x8	5x8	5x4	3.2x4	3.2x1.6	1.6x1.6	1.6x0.8	0.8x0.8
Requisite nodes for 1 run (nx x ny)	10x12 (=120)	20x12 (=240)	20x24 (=480)	30x24 (=720)	30x60 (=1800)	60x60 (=3600)	60x120 (=7200)	120x120 (=14400)
Requisite nodes for 100 ensemble runs	12k	24k	48k	72k	180k	360k	720k	1440k
Elapsed time of simulation by the double precision [sec]	128	56.6	30.2	20.5	10.9	7.90	4.86	3.97
Elapsed time of simulation by the single precision [sec] **(Estimated values)**	81	36	19	13	6.8	4.8	3.0	2.4

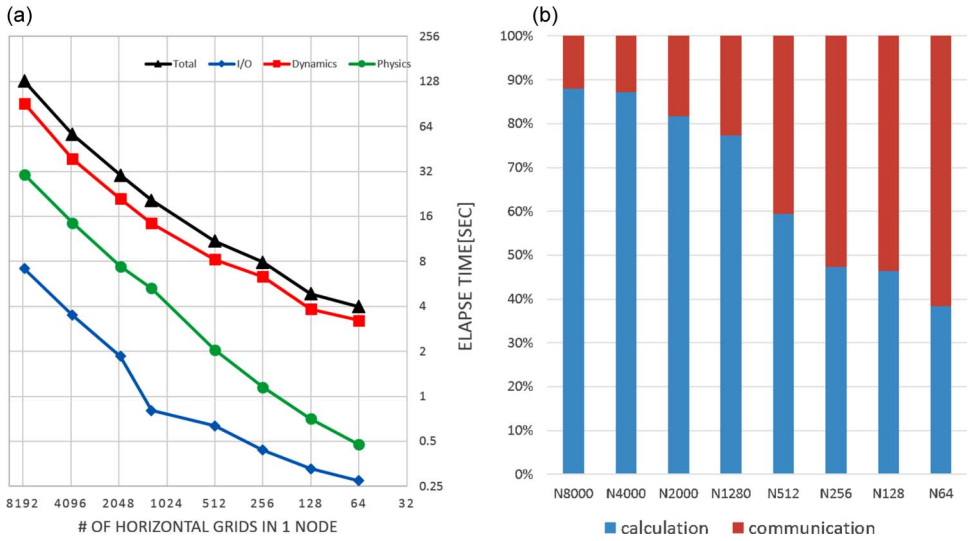

Fig. 11. *(a) Strong scaling of SCALE-LES. (b) Ratio of communication (red) to calculation (blue).*

domain size, resolution, and ensemble size, but before doing so, we propose to use single-precision variables in the model code instead of the default double precision. For geophysical modeling, using the double-precision variable is certainly safer. It is especially useful to avoid the violation of the conservation of mass and energy in a long-term climate simulation. However, using the single precision would not be too much harmful for a short range NWP in the BDA experiment. As shown in Table 3, the configuration N1280 requires 72000 nodes, less than the total node number of the K Computer.

The acceleration rate by changing the variable precision is shown in Table 4. Here, dynamics and physics correspond to dynamical core and physical processes (e.g., cloud microphysics and radiation), respectively. Although in this measurement the model configuration is different from the BDA configuration, this evaluation is fairly reasonable since the problem size in one node is smaller than N1280. The acceleration rate of the dynamical part is expected to be close to 2 because it is mainly limited by the memory bandwidth. The value of 1.81 is quite valid. On the other hand, the physical part tends to be the rate limiting of computation. The single-precision computing has the same peak performance as the double precision computing on the K computer, and the measured acceleration value of 1.27 would be understandable.

We can estimate the elapsed time with the single-precision variables as

$$T_a = T_{\mathrm{dyn}}/1.81 + T_{\mathrm{phys}}/1.27 + T_{\mathrm{io}}$$

where T_a is an estimated elapsed time with the single precision; and T_{dyn}, T_{phys}, and T_{io} are the measured elapsed times using the double precision for the dynamical process, physical process, and I/O, respectively. Note that I/O is already performed with the single precision even for the double-precision computing. The last row in Table 3 summarizes the estimated elapsed time with the single precision. The configuration case of N1280 satisfies the conditions of elapsed time and total number of nodes: The 100 ensemble runs of 30-s integration with 100-m horizontal resolution and 100 vertical levels in the 100 km squared domain could be finished within 13 s, using 72000 computer nodes of the K Computer. This performance expectation is very close to the goal of 10 s. It is also indicated in Table 3 that the 30-min single-member forecast can be finished within 3 min by

Table 4 Acceleration of Model Throughput Time by Single Precision

	Total time	Dynamics	Physics
Double precision[sec]	182.4	83.1	99.3
Single precision[sec]	124.1	45.9	78.2
Acceleration factor	1.47	1.81	1.27

the configuration of N128 with only 7200 nodes, much longer than the 30-s goal of BDA. As previously mentioned, the timing requirement of the 30-min forecast run is not as strict because it is separated from the cycling DA process. Even if we cannot meet the 30-s timing requirement, we could consider getting outputs earlier, for example, issuing the 10-min forecast within 1 min, while the 30-min forecast is still running.

V. BIG DATA TRANSFER

A. Mechanism of Direct Data Transfer

The NWP model (SCALE) and DA (LETKF) components in the current SCALE-LETKF workflow exchange information through file I/O operations using the global parallel file system. Historically, there have been mainly two reasons for this decision. First, the amount of transferred data is huge (it exceeds a terabyte in the target problem of BDA). Second, these models are being developed and maintained by independent groups; therefore, it has been strongly desired not to modify either of the component models when building a coupled system. While existing coupling toolkits, such as [16], could be utilized, they usually require significant modifications to the applications. Furthermore, data transfer via the global file system is easy and acceptable for systems without strict time constraints.

On the other hand, one of the SCALE-LETKF system's primary objectives is to provide real-time severe weather forecasting of sudden heavy rainstorms. This is by nature a strictly time-constrained procedure, and we find that file I/O-based data transfer between the SCALE and LETKF components is one of the hindering factors for acquiring real-time-ness. For the purpose of reducing data transfer time between the simulation and the DA steps, we have been developing a novel I/O middleware that supports direct data transfer between these two components. This section describes the design and implementation of our prototype I/O middleware, which supports direct parallel data transfer between workflow components, and thus, it can potentially accelerate forecasting of local severe rainstorms.

1) System Architecture: As we mentioned before, the SCALE-LETKF repeats a two-step cycle of NWP model simulation and DA, performed by two separately developed software, i.e., SCALE and LETKF. The I/O communication of one cycle in the current SCALE-LETKF system is depicted in Fig. 12(a). The Network Common Data Form (netCDF; http://www.unidata.ucar.edu/software/netcdf/) output data of the model simulation processes are first written to the global file system, which in turn are read by the DA processes. To put it from another angle, in each simulation step, the NWP model calculates possible atmospheric states in the future for every grid point in the 3-D space, where each atmospheric state is represented as a set of variables such as temperature and pressure. The model generates a large amount of output data, written in the netCDF format, which is requested by the subsequent DA step of the same cycle. In brief, the output data generated by the simulation process will be used by the corresponding DA process, which indicates the I/O communication takes place between process pairs.

To reduce the time needed for data transfer, we have been developing a novel I/O middleware to allow direct parallel data transfer between the two components. Fig. 12(b) illustrates the workflow of the system when the I/O middleware is utilized. In each cycle, the output data of simulation processes are directly forwarded to the DA processes, as well as the analyzed results generated

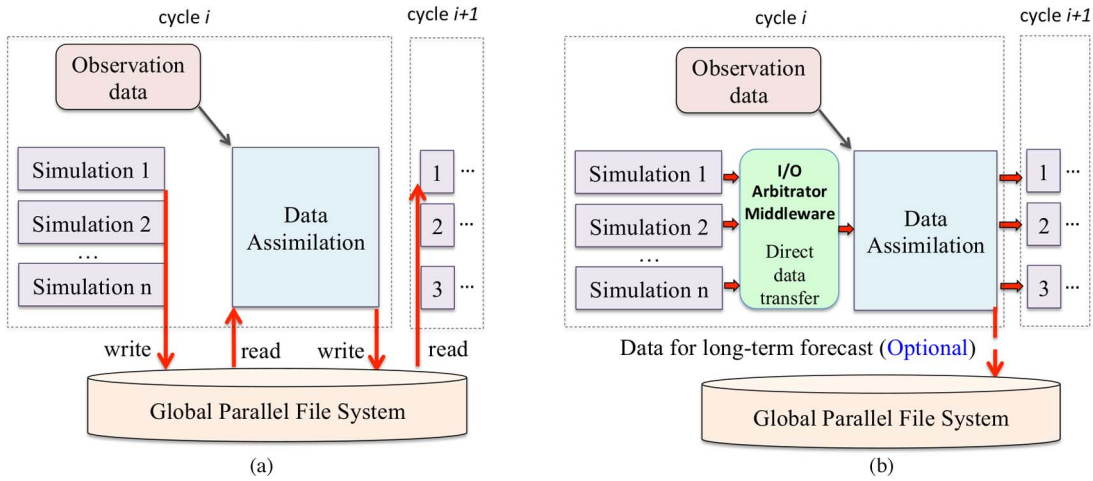

Fig. 12. *The communication pattern of one cycle in the SCALE-LETKF system utilizing (a) file I/O, or (b) direct data transfer.*

by DA processes which can be directly transferred to the simulation processes in the next cycle. Specifically, the I/O middleware connects the two processes by using MPI communication [5], and consequently, it enables direct communication between the model simulation processes and the DA processes. The following section describes the details of establishing a communication environment between the two kinds of processes.

2) Establishing Communication: Because the model and DA are separately developed applications, and are executed as separate MPI jobs, they do not share by default the same MPI communicator. To overcome this problem, our prototype implementation currently utilizes the standard MPI intercommunicator family of routines to establish a communication context between the two types of jobs. Fig. 13 demonstrates the details of this approach.

At initialization time, the server process, i.e., a DA process opens a port using the *MPI_Open_port* feature, and then publishes it by using *MPI_Publish_name*. Subsequently, the connection thread of each individual DA process waits in *MPI_Comm_accept*. The connection service is expected to be already running by the time the client processes attempt to build the connection. Client processes, i.e., processes of the model simulation component, can connect to the server processes with *MPI_Comm_connect* once they successfully obtained the service name by using the *MPI_lookup_name* function. As a result, processes of both components can communicate with each other by using standard MPI functions. After the data transfer took place, the client processes proactively disconnect and the server processes can unpublish their connection services with *MPI_Unpublish_name*.

3) Middleware Implementation for SCALE-LETKF: For demonstrating the effectiveness of point-to-point direct communication between the simulation and DA processes in SCALE-LETKF, we have developed a proof-of-concept implementation of the proposed I/O middleware. In addition, since data are exchanged between each SCALE process and the corresponding LETKF process in netCDF format, we have made slight modifications to the netCDF library itself (using ver. 4.2.2.1) so that it complies with the proposed I/O middleware to enable direct data transfer in an application transparent fashion.

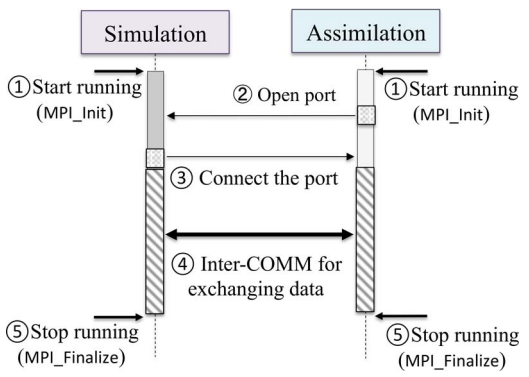

Fig. 13. ***Establishing communication between the two workflow components.***

B. Computational Performance

This section first describes the experimental settings and experimental methodology for evaluating the proposed I/O middleware. It then presents experimental results and provides the relevant discussion. For more details, refer to Liao *et al.* [17].

1) Experimental Setup: Experiments to assess the advantages of the SCALE-LETKF system equipped with our current prototype middleware were conducted on the K computer. As for the input data used in our experiments, we use the SCALE-LETKF to perform the data assimilation cycle for regional weather analysis employing real-world observations to test the efficiency when equipped with the proposed I/O middleware. Note that in these tests, the domain size is bigger but the grid resolution and problem size are much lower than the target BDA system. We expect that the I/O middleware will be much more beneficial when applied to the BDA system because of its larger amount of I/O size. Here the following two test cases were conducted:

- EXP_L36
  - grid numbers per member: 90 (east-west) × 90 (north-south) ×36 (vertical);
  - number of variables at one grid: 11;
  - ensemble size (number of ensemble members): up to 100;
  - total variable number: $90 \times 90 \times 36 \times 11 \times$ (up to 100) = up to 3.2×10^8;
  - number of processes: up to 400 (four per members);
  - total I/O size: (77.8 + 8.9) MB per processes, up to 35 GB for the entire 100 members;
- EXP_L72
  - same as EXP_L36 but with doubled (72) vertical layers;
  - total variable number: up to 6.4×10^8;
  - total I/O size: (151.8 + 16.2) MB per processes, up to 67 GB for the entire 100 members.

In each measurement, SCALE is composed of up to 100 ensemble instances, with four processes in each ensemble instance. LETKF consists of only one instance, but it contains the same number of processes as all SCALE instances is total.

2) Experimental Results: We test one cycle of the SCALE-LETKF; i.e., each SCALE process generates

output data after data simulation, which data will be read by the corresponding LETKF process as the input data for assimilation. For comparison, we record the time required for transferring data between the SCALE and LETKF processes by using file-based I/O operations and the mechanism of direct data transfer. Scaling the number of ensemble SCALE instances from 10 to 100, Fig. 14(a) and (b) demonstrates the time required for transferring data between the two kinds of processes utilizing file I/O and the proposed middleware.

As Fig. 14 shows, the proposed mechanism can greatly reduce the time needed for transferring the data between SCALE and LETKF processes compared to the file I/O-based data transfer. For example, when the ensemble size is 100 in the EXP_L72, the mechanism of direct data transfer can reduce the I/O time by 82.7%, which implies that more time can be devoted to perform model and DA applications. Furthermore, file based data transfer may require significantly increased I/O time due to contention on the parallel file system. The EXP_L72 caused 34.1% more time for transferring the data, compared with the EXP_L36, because the size of transmission data needed by the former case is twice as large as that of the latter case. In contrast, direct data transfer does not increase significantly for transferring double size of data.

3) Summary and Discussion: With respect to comparing direct data transfer and file-based I/O, we emphasize the following two key observations. First, with increasing number of processes direct data transfer yields better relative performance. Second, more time reduction can be achieved with the growing size of the transferred data. In brief, we conclude that the proposed file I/O middleware can significantly reduce the time required by exchanging data between the component models in the SCALE-LETKF workflow system.

Furthermore, our I/O middleware offers a general framework for intercomponent data exchange in workflow systems, where individually developed applications are coupled together. By accelerating the execution of such systems, we believe the newly proposed middleware having the direct data transfer functionality is particularly important for systems with rigorous time constraints.

We note that the current proof-of-concept I/O middleware is only applicable to run only one cycle of the SCALE-LETKF. Extending the I/O middleware tool to multiple data assimilation cycles is ongoing work. Besides, to perform the real-time weather analysis and forecasting using the data generated by satellites and radars, the SCALE-LETKF includes another kind of application (named "observation operator") for computing the observational values in the short-term model forecasts. Therefore, the I/O middleware needs to transfer observation data directly among more different components. Fig. 15 illustrates the entire I/O flow of SCALE-LETKF by employing the proposed I/O middleware, which will be implemented and put into practice in the near future.

VI. CASE STUDIES

Here we demonstrate the short-term forecasts of two rainfall cases using the prototype system we have developed to realize the idea of BDA. These two cases occurred in Japan's Kansai region and were well observed by the Osaka University PAWR, exhibiting distinct types of convective systems. We performed all of the Big Computations on the K computer.

The components of the prototype BDA system have been described in the previous sections, including the PAWR observations (Section III-A: observational big data), the high-resolution NWP models (Section IV: Big Simulation), and the communication between the

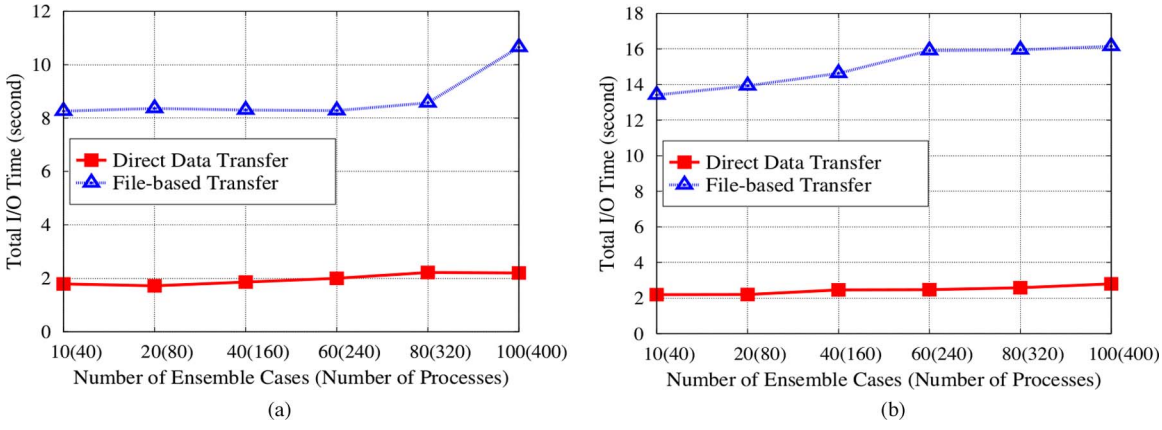

Fig. 14. *Data transfer time utilizing file I/O and direct data transfer. (a) EXP_L36 and (b) EXP_L72.*

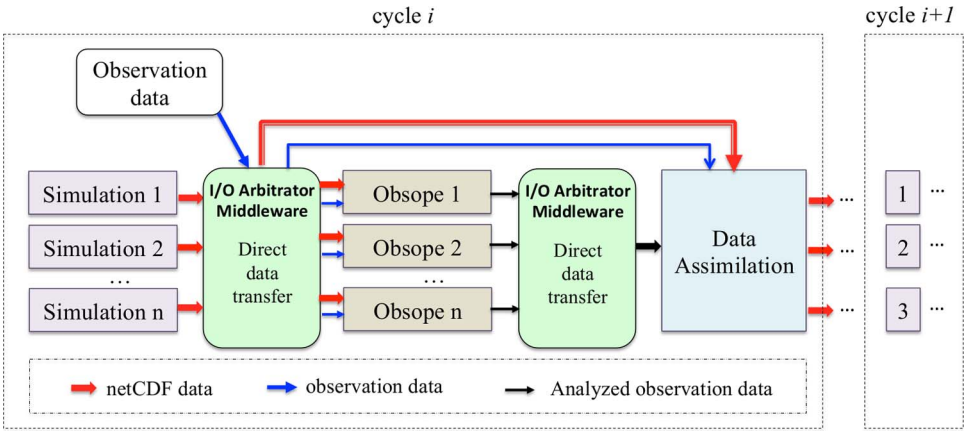

Fig. 15. *I/O flow in the future SCALE-LETKF system with direct data transfer.*

radar site and the computer and the I/O middleware (Section V: big data transfer). Now we reached the middle stage of the system development: The current system has been ready for use to conduct retrospective experiments with the targeted problem size, but the direct data transfer mechanism has not been fully employed yet, and the total computational time of all components has not been fast enough to perform real-time applications. To reach the goal, the development by each subgroup is actively ongoing. Besides, for the NWP model component, we test here not only the newly developed SCALE model, but also the JMA nonhydrostatic model (JMA NHM, [34]) which is similar to the SCALE model but a matured operational model used in JMA to produce routine operational mesoscale forecasts. JMA NHM has also been coupled to the LETKF, named NHM-LETKF, by Miyoshi and Aranami [19] and Kunii [15]. The performance of the NHM-LETKF system will be a useful reference for the SCALE-LETKF experiments.

The NWP-based BDA method relies on an NWP model that solves the geophysical fluid dynamics equations with complicated atmospheric physical processes, and on a DA method that bridges the model forecasts and the observations to find the most probable state based on their error statistics. In addition to the NWP and DA approach, we also developed a simpler "nowcasting" system based on the 3-D space-time extrapolation of the high-density PAWR data [30]. This method does not solve the sophisticated physical equations but instead calculate the rainfall prediction assuming linear motion of the convective cells within a short forecast time. Similar methods have also been commonly used in many operational weather forecast centers to assist their warning of heavy rainfall. For example, JMA operates the High-Resolution Precipitation Nowcasts (HRPN) at 250-m resolution and provides the precipitation forecast for the next hour in real time [13]. Our experimental nowcasting system explored the technique at much higher resolution by taking advantage of the PAWR and K computer. We also computed the space-time extrapolation in three dimensions, which showed clear advantage over the traditional 2-D method [30]. In this section, we present the results from the nowcasting approach in comparison to the NWP-based BDA results.

A. Kyoto Case on July 13, 2013

The first case is an afternoon thunderstorm case on July 13, 2013 [Fig. 16(a)]. Afternoon thunderstorms are common phenomena during the summer time, developing under an unstable environment condition with the ground surface heated by the sun. Many afternoon thunderstorms are small and dissipate quickly, but under a favorable condition, the storms can be particularly strong and well organized, and may affect human activities. Not only do the large-scale environment and solar heating control the genesis and development of the afternoon

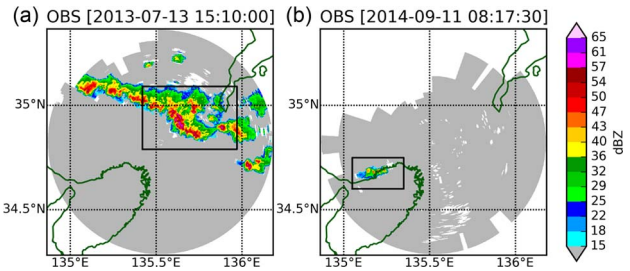

Fig. 16. *Reflectivity (dBZ, color shades) observed by Osaka University PAWR for (a) Kyoto rainfall case at 15:10:00 LT July 13, 2013 at 4-km height, and (b) Kobe rainfall case at 08:17:30 LT September 11, 2014 at 2-km height. The gray and white shaded areas correspond to the radar observation coverages and missing data, respectively. The black rectangles in (a) and (b) indicate the zoom-in regions shown in Figs. 2 and 3, respectively. The plotted area corresponds to the model calculation domain.*

thunderstorms, but also the local circulation and inhomogeneous heating caused by the terrain play roles in these processes. Therefore, to make accurate model prediction of these systems, having a high-resolution model resolving the fine-scale temperature and circulation fields is important. Also, DA of high-resolution observations such as the PAWR data to construct an accurate initial condition at small scales is very important.

We perform retrospective forecast experiments using all available tools mentioned above, including the NWP method using the NHM-LETKF and SCALE-LETKF assimilating the PAWR data, and the space-time extrapolation from the PAWR data (hereafter EXTRAP). The experimental design is summarized in Table 5. For this case, all radar coverage (120 × 120 km) in a horizontal plane are included in the simulation and forecasts. For the NWP methods, we use 60 (98) terrain-following vertical levels from the surface to 20 km (26 km) elevation in NHM-LETKF (SCALE-LETKF). Eleven atmospheric variables (3-D wind components, temperature, pressure, mixing ratios of water vapor, cloud water, cloud ice, rain, snow, and graupel) are represented at each grid point, and 100 ensemble simulations are conducted. These multiple dimensions make the problem size extremely big: it amounts to about $O(10^{11})$ variables in total.

The NWP methods need a certain period of multiscale spinups. For NHM-LETKF, we first run a broader domain at 15-km resolution, assimilating global conventional observation data, and then we initiate the second 1-km-resolution domain at 12:00:00 Japanese local time (LT; UTC+9), July 13, 2013. Finally, the 100-m-resolution BDA study domain (Fig. 16) is the third domain initiated at 14:30:00 LT, 30 min before the DA of the PAWR data starts at 15:00:00 LT. After 20 cycles for 10 min, a 30-minute deterministic forecast is initialized from the ensemble mean analysis at 15:10:00 LT. For SCALE-LETKF, a similar multiscale strategy is employed with four domains at 15-km, 5-km, 1-km, and 100-m resolution, respectively. The outermost domain at 15-km resolution is set up in the same way as the NHM-LETKF. The second, third, and fourth domains are initiated at 09:00:00 LT July 12, 11:00:00 LT July 13, and 15:00:00 LT July 13, respectively. The timing of the 100-m cycling analysis and forecast in the fourth study domain is the same as that in the third domain of NHM-LETKF. The QC process of the PAWR data follows Ruiz *et al.* [33], and the detailed experimental design for the NHM-LETKF experiment was described by Miyoshi *et al.* [23]. Using the NWP models, we can obtain full-field values in the calculation domain at all grid points for all 11 atmospheric variables, not limited to the observed radar reflectivity.

Table 5 Settings of the NHM-LETKF, SCALE-LETKF, and Extrapolation Experiments. Times Shown in the Table Are the Japanese Local Time. For the NHM-LETKF and SCALE-LETKF Experiments, Only the Settings for the Study (Innermost) Domains Are Listed

Experiment		Data dimensions					Period	
System	Case	Horizontal grids (domain size)	Vertical grids	Variables	Ensemble	Total	Cycling DA analysis	Forecast
NHM-LETKF	July 13, 2013	1201×1201 (120×120 km)	60	11	100	9.5×10^{10}	10 min (15:00:00-15:10:00)	30 min (15:10:00-15:40:00)
	September 11, 2014	1201×1201 (120×120 km)	50	11	100	7.9×10^{10}	17.5 min (08:00:00-08:17:30)	10 min (08:17:30-08:27:30)
	September 11, 2014 (1 km)	121×121 (120×120 km)	50	11	100	8.1×10^{8}	32.5 min (07:45:00-08:17:30)	10 min (08:17:30-08:27:30)
SCALE-LETKF	July 13, 2013	1200×1200 (120×120 km)	98	11	100	1.6×10^{11}	10 min (15:00:00-15:10:00)	30 min (15:10:00-15:40:00)
EXTRAP	July 13, 2013	1201×1201 (120×120 km)	100	1	1	1.4×10^{8}	N/A	10 min (08:17:30-08:27:30)
	September 11, 2014	350×250 (35×25 km)	100	1	1	8.8×10^{6}	N/A	10 min (08:17:30-08:27:30)

As for the extrapolation method (EXTRAP), we use 100 Cartesian coordinate vertical levels from 0 to 10 km. This method simply takes the PAWR reflectivity observation at 15:10:00 LT as the initial condition, calculates the motion vectors using the observation at the previous time (15:09:30 LT), and then advect the reflectivity field by the motion vectors for the subsequent 30 min. QC of the PAWR data and a step to fill the missing values are performed before the computation [30]. Unlike the NWP methods, EXTRAP does not require a spinup procedure. Besides, the problem size is much smaller because we only consider the 30-min forecast of the 3-D reflectivity field without knowing the other atmospheric variables. An ensemble is not needed, either.

The reflectivity observations show an organized strong convective rainband [Fig. 16(a)]. Using the NWP and extrapolation forecast systems described above, the forecast results within the black rectangle zoom-in area are shown in Fig. 17. The initial conditions for the dynamical models [Fig. 17(b) and (c)] are the optimal estimates from the DA process. Since the model reflectivity fields [Fig. 17(b) and (c)] closely resemble the observation field [Fig. 17(d)], we are confident that the prototype BDA system keeps the simulated state very close to the actual observations. For EXTRAP, the initial condition [Fig. 17(a)] is the same as the observations except that the missing data are filled. During the 30-min forecast period, the observed convective system generally moves eastward following the large-scale mean flow, but it also evolves quickly and keeps changing its intensity and shape. EXTRAP predicts the movement of the system and roughly conserves the intensity of the rain. It performs well in the first few minutes, but beyond that, it has no chance to predict the newly developed convective cells [30]. Apparently, the EXTRAP forecast becomes less realistic in the later time, indicating the fundamental limitation.

By contrast, the NHM-LETKF and SCALE-LETKF forecasts show not only the movement but also the development of the rain system. NHM-LETKF shows an exceedingly strong big convective cell in the eastern side of the domain [Fig. 17(f), (j), (n), and (r)], whereas

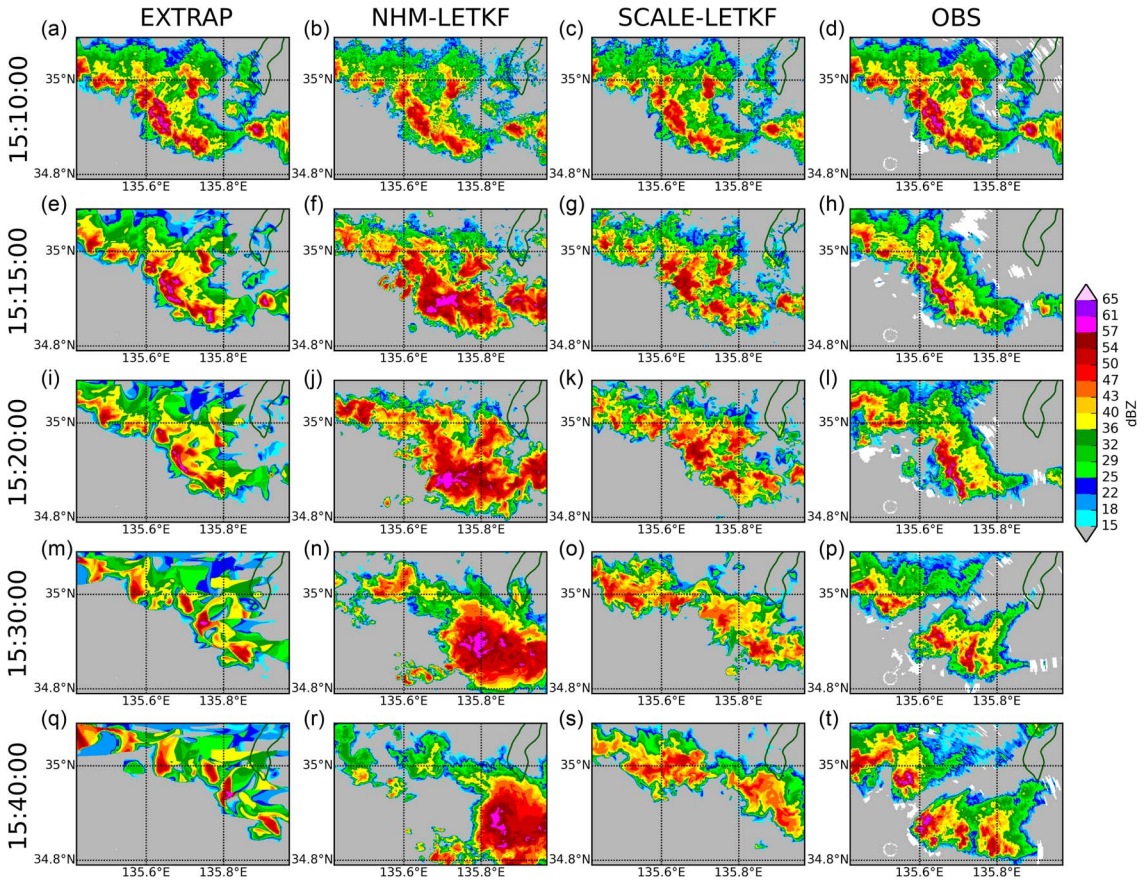

Fig. 17. ***The model forecast results (EXTRAP, NHM-LETKF, and SCALE-LETKF) compared with observations (OBS) for the July 13, 2013 case in the zoom-in region in Fig. 16(a). The color shades show reflectivity (dBZ) at (a)–(d) forecast initial time (15:10:00 LT); (e)–(h) 5-min forecasts; (i)–(l) 10-min forecasts; (m)–(p) 20-min forecasts; and (q)–(t) 30-min forecasts, except that the rightmost column indicates actual PAWR observation as the verification truth. The white areas in PAWR observations indicate missing data.***

SCALE-LETKF shows reasonably good structure of the northwest–southeast oriented convective rainband [Fig. 17(g), (k), (o), and (s)]. Comparing the precipitation patterns of the 30-min forecasts from EXTRAP, NHM-LETKF, and SCALE-LETKF [Fig. 17(q)–(s)], we find that the SCALE-LETKF forecast corresponds most accurately to the observation [Fig. 17(t)]. Besides, based on the dynamical and physical processes in which all atmospheric variables are involved, the NWP models have the potential to predict the newly generated convective cells under a specific 3-D condition. However, the accurate prediction of individual convective cells is really challenging.

Without the high-resolution model and the dense and frequent PAWR data, we could do nowhere close to the results we have obtained so far. However, the forecast results from the prototype BDA systems for each individual convective cell are still far from ideal. The inaccurate prediction would be related to the challenges both in modeling and in DA, and may be caused by several possible reasons as follows.

1) The 10-min period of the DA cycling may be too short. The 20 data assimilation cycles may not be sufficient to adjust the model field toward the observed atmospheric conditions. It is essential to have a good representation of the error covariance in the ensemble, but it takes time to develop. DA experiments with longer periods need to be studied.
2) The strong adjustment within a short time may cause dynamical imbalance. The analyses can be forced to be very close to the observations, but many of the individual convective cells in the model forecast gradually dissipate. This is a common problem of the mesoscale radar assimilation [45].
3) We use the ensemble mean analyses over the 100 members to initialize the deterministic forecasts. Although the ensemble mean provides the most probable state of the ensemble Kalman filter, the average may cause dynamic imbalance due to the imperfect assumptions of the linear dynamics and Gaussian statistics. Choosing one or a subset of the ensemble members as the initial conditions may avoid the potential problem.
4) The model may not have been well tuned at this high resolution, especially for the JMA NHM that is designed for the operational weather forecast at kilometer scales, not for DA at 100-m resolution. This is one of the reasons why we decided to use the newly developed SCALE model as one of the central components of the BDA project. The SCALE model, as described in Section IV, is designed to be more suitable for subkilometer-scale simulations. Although the development of SCALE is still at an early stage, it has already shown advantages over the JMA NHM. Continuous efforts will be made to improve the model performance for the targeted problem of BDA. One of our important plans is to use the LETKF to adaptively estimate the tuning parameters of the model physics (e.g., [32]).

B. Kobe Case on September 11, 2014

The second case is an event of isolated convective cells generated in the morning on September 11, 2014, in Kobe, where the K computer is located [Fig. 16(b)]. This kind of sudden rainfall event has an impact on people's activities, but it is even harder to forecast those events since there is no sign before it appears. Besides, the size of the convective system is small (~10 km), so that it is hardly resolved in the current operational NWP system with a-few-kilometer resolution. Here we attempt to simulate and make the retrospective forecast of this difficult event using the EXTRAP and NHM-LETKF systems. As summarized in Table 5, for this case, we run the NHM-LETKF system with the procedure similar to the first case, but using 50 vertical levels. For the multiscale spinup, we first run the outermost domain at 15-km resolution with conventional observation data for more than ten days from September 1, 2014, and initiate the second domain at 5-km resolution at 03:00:00 LT, September 11, 2014. The third domain at 1-km resolution is downscaled from the second domain at 06:00:00 LT, providing the boundary conditions for the study domain [the fourth domain, Fig. 16(b)] initiated at 07:45:00 LT at 1-km resolution. After 15-min cycling DA at 1-km resolution for the study domain with the PAWR data until 08:00:00 LT, the resolution is switched to 100 m, and the cycling DA continues at 100-m resolution. Here, the boundary conditions are provided by the third domain at 1-km resolution. Finally, a 10-min deterministic forecast is initialized from the ensemble mean analysis at 08:17:30 LT. For comparison, an additional 1-km-resolution DA and forecast experiment is performed by replacing the 100-m-resolution model with the 1-km-resolution model. The EXTRAP experiment uses a smaller domain with 350 × 250 horizontal grid points (35 × 25 km), only covering the area affected by the small convective system, since in this case the extrapolation calculation result will be the same with the entire 120- × 120-km domain.

The observed radar reflectivity at 08:17:30 LT at 2-km height is shown in Fig. 16(b). The results within the black rectangle zoom-in area are shown in Fig. 18. At the forecast initial time (08:17:30 LT, the top row), the PAWR observation shows four separate small convective cores [Fig. 18(d)], and the NHM-LETKF represents these fine structures very well at 100-m resolution but not at 1-km resolution [Fig. 18(b) and (c)]. The EXTRAP directly uses the PAWR observation as the initial condition [Fig. 18(a) and (d)]. In this

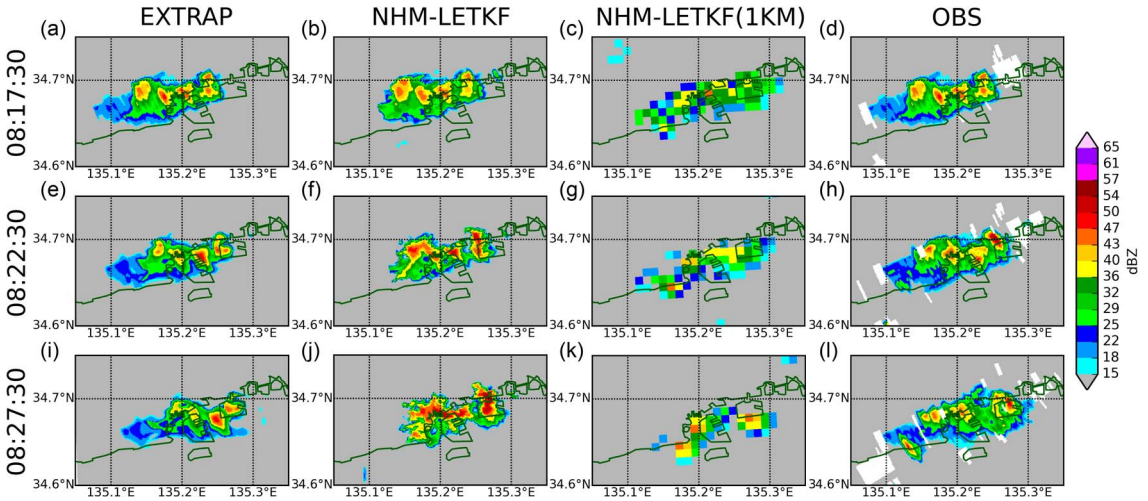

Fig. 18. *Similar to Fig. 17, but including the 1-km resolution results (c), (g), (k) for the September 11, 2014 case in the zoom-in region in Fig. 16(b). The color shades show reflectivity (dBZ) for (a)–(d) the forecast initial time (08:17:30 LT); (e)–(h) 5-min forecasts; and (i)–(l) 10-min forecasts.*

case, the EXTRAP maintains a relatively good forecast in the first 5 min but fails to track each individual cell after that. The NHM-LETKF experiment at 100-m resolution predicts the four convective cells better than EXPRAP during the 10-min forecast and reveals the growing trend of this newly developed system, although they become slightly too strong and too compact compared to the observation [Fig. 18(f) and (j)]. The results demonstrate the potential usefulness of the BDA system on forecasting such a sudden convective rainfall case, which is beyond the scope of the current NWP systems. The results also highlight the advantage of the 100-m resolution model and DA.

C. Computational Performance

The computational time and the amount of total floating-point operations (FLOP) of the NHM-LETKF and SCALE-LETKF systems are listed in Table 6. As mentioned before, we have not fulfilled the real-time requirement, as the wall-clock time of the computations for a 30-s cycle is much longer than 30 s. Note that the K computer has about 80 000 nodes (eight cores per node) and we have not used the full system to perform the experiments. To be able to efficiently utilize the full system, many components need to be improved, including those described in the previous sections. For example, based on the profiler data and the diagnostic outputs from each program, we learned that the disk I/O consumed a large portion of the computational time when many nodes are used, so that a considerable improvement by using the I/O middleware described in Section V is expected.

We are in the middle stage of the project, and many components that have been developed separately by each group are going to be integrated with further adjustments and developments. Therefore, these numbers

Table 6 Computational Time and the Total Floating Point Operations of One Data Assimilation Cycle for NHM-LETKF and SCALE-LETKF. The Number of Floating-Point Operations Are Measured by the K Computer Profiler Software

System	Nodes × seconds (floating-point operations)		
	Cycling analysis		Forecast
	100 parallel 30-second simulations	Data assimilation	A single 30-minute simulation
NHM-LETKF	4800 nodes × 274 s (2.6×10^{15})	1536 nodes × 1453 s (4.5×10^{15})	196 nodes × 10600 s (1.6×10^{15})
SCALE-LETKF	4352 nodes × 1964 s (3.3×10^{16})	4352 nodes × 1106 s (6.2×10^{15})	256 nodes × 12200 s (2.0×10^{16})

show the current baseline of the system that is expected to be greatly improved in the future. We are going to explore how much we can achieve using the full capacity of one of the world's leading-edge supercomputers, and to design a possible future BDA system in the upcoming post-petascale era.

VII. POTENTIAL USE OF HIMAWARI-8

The previous section presented the most recent results of the current prototype BDA system using the PAWR data every 30 s. In addition, the potential use of Himawari-8 data has been explored in parallel. This section describes the potential use of Himawari-8 in the BDA system.

A. Rapid-Scan AMV

The BDA project aims to improve the forecast accuracy of local heavy rainfalls by assimilation of high-frequency and high-density observation data. Here, the environmental conditions such as large-scale low-level horizontal convergence and upper level cold airflow at an O(10 km) scale or larger (also known as the meso-β scale, or the horizontal scale of a group of convection cells) are important. For example, if the cold airflow in the simulated state before DA is inaccurate and, say, too intense, the observed thunderstorm area is preoccupied by the intense cold airflow and cannot be completely corrected by the assimilation of PAWR data that provide detailed observations about individual convective cells. In this case, the large-scale representation of warm and cold air convergence is essential for simulating the local thunderstorms accurately.

The rapid-scan AMV data from Himawari-8 (Section III-B) will be potentially useful to improve the meso-β and larger scale phenomena including large-scale convergence. Not having tested with the improved Himawari-8 AMVs yet, but Otsuka *et al.* [29] explored the usefulness of the rapid-scan AMVs in a heavy rainfall case on August 13, 2012 using the MTSAT-1R data. They used the JMA operational DA system known as JNoVA (JMA Non-hydrostatic Variational DA system, [7]) and included the additional rapid-scan AMVs. The results showed overall positive impact on representing meso-β scale phenomena. This is encouraging for BDA, so that the improved Himawari-8 AMVs would be useful to obtain better environmental condition for the 100-m mesh BDA system.

B. Brightness Temperature

In addition to the AMV data, we have been exploring effective data assimilation methods for infrared brightness temperature from Himawari-8. The brightness temperature obtained by rapid scan observation is expected to be used for the forecasts of local heavy rainfalls, as it provides the information of moisture flows and surface temperature in the clear-sky regions, and in cloudy regions, it may capture the generations of convection cells before PAWR captures large raindrops. At an early stage of convective development, only small cloud particles exist, and large raindrops grow at a later stage. Radars are sensitive to larger raindrops, and we would expect Himawari-8 can complement the PAWR data by capturing initiating clouds at an earlier time. In this project, the assimilation method of clear-sky and cloud-affected brightness temperature for the forecasts of local heavy rainfalls is being developed.

Brightness temperature observations in the clear-sky regions and only those from cloud-unaffected bands in cloudy regions have been used in most operational DA systems. Interestingly, only the bands that are not sensitive to clouds are used in cloudy regions because using cloud-affected brightness temperature is very difficult with current DA systems. This is somewhat ironic since what we see with our eyes are clouds in the satellite image. Therefore, we explore using cloud-affected brightness temperature observations. The simplest approach assumes opaque, uniform single-layer clouds. Okamoto [26] developed a method to incorporate the single-layer cloud model in a radiative transfer calculation and evaluated its impact on the JMA operational global data assimilation system. However, this approach may not be appropriate in BDA since high-resolution simulations in BDA should include detailed representations of different types of clouds beyond what are represented by the simplified single-layer cloud model.

Therefore, we are developing a new approach to assimilate the brightness temperature observations in more general cloud regions including multilayer clouds. As the first step, the outputs of JMA NHM forecasts were compared with the observation data of Himawari-8. Fig. 19 shows brightness temperature observed by Himawari-8 on April 10, 2015 and those simulated by JMA NHM with the grid intervals of 2 and 5 km. The results show general agreement between the simulation and actual observation. If we look carefully, we find that the simulated brightness temperature from high clouds of developed convection cells are not cold enough. The 2-km resolution simulation provides slightly better brightness temperature of developed convection cells, but overall, 2- and 5-km results show similar patterns.

We are working on estimating the observation error and bias of the cloud-affected brightness temperature to develop QC procedures dependent on cloud effect following Okamoto *et al.* [27], and to conduct the DA experiments to explore the potential usefulness of brightness temperature in BDA.

VIII. FUTURE PERSPECTIVE

This paper presented the concept of BDA, how the "science big data" from the new-generation sensors and highest end supercomputing could possibly bring

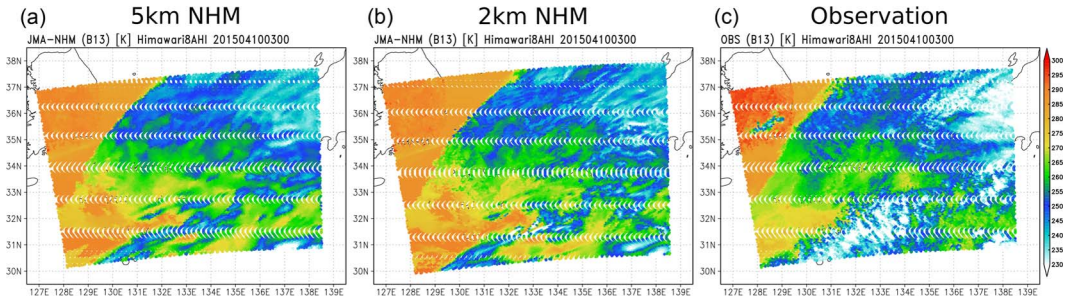

Fig. 19. ***Brightness temperature (K) of Himawari-8 band 13 at 0300 UTC April 10, 2015 for (a) 3-h forecasts of JMA NHM at 5-km grid spacing; (b) at 2-km grid spacing; and (c) Himawari-8 observation.***

revolution to NWP, with detailed descriptions on PAWR, Himawari-8, big simulation, and big data transfer. The revolutionary BDA system aims to update every 30-s weather forecasting pinpoint at 100-m resolution, orders of magnitude more rapidly and more precisely than the current routine systems. This type of frequent and precise weather forecasting would be relevant to our preparedness for sudden local severe weather such as tornadoes, flash floods, and lightning strikes. To explore the BDA concept, we developed two prototype BDA systems, NHM-LETKF and SCALE-LETKF, and the results for two retrospective cases showed potential usefulness and effectiveness of the high-resolution weather forecasting although there is room for improvement. In particular, the results suggest that the local heavy rainfall forecasting need substantial improvement through developing the NWP model including complex cloud microphysics and DA methods for the frequent and high-resolution updates. In addition, we have a big challenge in the real-time-ness. The computational performance including the I/O procedure at this moment is not satisfactory to enable the 30-s updates even with the 10-petaflops K computer. The Japan's flagship 2020 project is currently ongoing to develop a post-petascale supercomputer in 2020. Based on what we learn from the K computer, we plan to design the BDA system toward the post-petascale era. The scope includes a multiscale system design from the global scale to the local storm scale and the exploration of a big ensemble (e.g., [21] and [22]) to fully utilize the big data from different sources. Although our BDA effort so far is limited to so-called "science big data," the power of big data is expanding far beyond. We will keep exploring frontiers of using big data beyond what has been explored. ■

Acknowledgment

T. Miyoshi is the lead PI of the entire project, is the main author of Sections I, II and VIII, and supervised the development of the entire manuscript with G.-Y. Lien. G.-Y. Lien performed the SCALE-LETKF experiments and is the main author of Section VI. S. Satoh and T. Ushio are Co-PIs of the project and are the main authors of Section III-A. K. Bessho is the main author of Section III-B. H. Tomita is a Co-PI of the project and is the main author of Section IV with S. Nishizawa, R. Yoshida, and S. A. Adachi. Y. Ishikawa is a Co-PI of the project and is the main author of Section V with J. Liao and B. Gerofi. M. Kunii performed the NHM-LETKF experiment in Section VI-A. J. Ruiz contributed to the experiments in Section VI. Y. Maejima performed the NHM-LETKF experiment in Section VI-B. S. Otsuka performed the EXTRAP experiments in Section VI. M. Otsuka, K. Okamoto, and H. Seko are the main authors of Section VII. All authors read and approved the final manuscript.

The PAWR data were archived in the NICT Science Cloud and made available to public through http://pawr.nict.go.jp/. The numerical experiment results were archived locally at RIKEN Advanced Institute for Computational Science (AICS), Kobe, Japan. The LETKF data assimilation FORTRAN90 code is based on the publicly available code at https://github.com/takemasa-miyoshi/letkf. The JMA NHM model code was provided by JMA under the cooperative research contract between RIKEN and MRI. Numerical Prediction Division of JMA provided initial and boundary conditions and operational observation data. Part of the results was obtained by using the K computer at the RIKEN AICS through proposal numbers ra000015, hp150019, and hp160162.

REFERENCES

[1] K. Bessho *et al.*, "An introduction to Himawari-8/9-Japan's new-generation geostationary meteorological satellites," *J. Meteorol. Soc. Jpn.*, vol. 94, pp. 151–183, 2016, DOI: 10.2151/jmsj.2016-009.

[2] H. B. Bluestein, M. M. French, I. PopStefanija, R. T. Bluth, and J. B. Knorr, "A mobile, phased-array Doppler radar for the study of severe convective storms: The MWR-05XP," *Bull. Amer. Meteorol. Soc.*, vol. 91, pp. 579–600, 2010, DOI: 10.1175/2009BAMS2914.1.

[3] W. Chang, K.-S. Chung, L. Fillion, and S.-J. Baek, "Radar data assimilation in the Canadian High-Resolution Ensemble Kalman Filter system: Performance and verification with real summer cases," *Monthly Weather Rev.*, vol. 142, pp. 2118–2138, 2014, DOI: 10.1175/MWR-D-13-00291.1.

[4] M. Goldberg *et al.*, "The global space-based inter-calibration system," *Bull. Amer. Meteorol. Soc.*, vol. 92, pp. 467–475, 2011, DOI: 10.1175/2010BAMS2967.1.

[5] W. Gropp, E. Lusk, and A. Skjellum, *Using MPI: Portable Parallel Programming With the Message-Passing Interface*, 2nd ed. Cambridge, MA, USA: MIT Press, 1999.

[6] T. Hara *et al.*, "The operational convection-permitting regional model at JMA," *CAS/JSC WGNE Res. Activ. Atmos. Ocean. Model*, p. 5, 2013.

[7] Y. Honda and K. Sawada, "Upgrade of the operational mesoscale 4D-Var system at the Japan Meteorological Agency," *CAS/JSC WGNE Res. Activ. Atmos. Ocean. Model.*, pp. 1–11, 2009.

[8] B. R. Hunt, E. J. Kostelich, and I. Szunyogh, "Efficient data assimilation for spatiotemporal chaos: A local ensemble transform Kalman filter," *Phys. Nonlinear Phenom.*, vol. 230, pp. 112–126, 2007, DOI: 10.1016/j.physd.2006.11.008.

[9] B. Isom *et al.*, "The atmospheric imaging radar: Simultaneous volumetric observations using a phased array weather radar," *J. Atmos. Ocean. Technol.*, vol. 30, pp. 655–675, 2013, DOI: 10.1175/JTECH-D-12-00063.1.

[10] T. A. Jones, D. Stensrud, L. Wicker, P. Minnis, and R. Palikonda, "Simultaneous radar and satellite data storm-scale assimilation using an ensemble Kalman filter approach for 24 May 2011," *Monthly Weather Rev.*, vol. 143, pp. 165–194, 2015, DOI: 10.1175/MWR-D-14-00180.1.

[11] E. Kalnay, *Atmospheric Modeling, Data Assimilation, and Predictability*. Cambridge, U.K.: Cambridge Univ. Press, 2003, p. 368.

[12] H. H. Kieffer and T. C. Stone, "The spectral irradiance of the Moon," *Astron. J.*, vol. 129, p. 2887, 2005, DOI: 10.1086/430185.

[13] S. Kigawa, "Techniques of Precipitation Analysis and Prediction for High-Resolution Precipitation Nowcasts," The Japan Meteorological Agency, 2015. [Online]. Available: http://www.jma.go.jp/jma/en/Activities/Techniques_of_Precipitation_Analysis_and_Prediction_developed_for_HRPNs.pdf

[14] P. R. Krehbiel, and M. Brook, "A broad-band noise technique for fast-scanning radar observations of clouds and clutter targets," *IEEE Trans. Geosci. Electron.*, vol. 17, pp. 196–204, 1979, DOI: 10.1109/TGE.1979.294649.

[15] M. Kunii, "Mesoscale data assimilation for a local severe rainfall event with the NHM-LETKF system," *Weather Forecast.*, vol. 29, pp. 1093–1105, 2014, DOI: 10.1175/WAF-D-13-00032.1.

[16] J. Larson, R. Jacob, and E. Ong, "The model coupling toolkit: A new Fortran90 toolkit for building multiphysics parallel coupled models," *Int. J. High Perform. Comput. Appl.*, vol. 19, pp. 277–292, 2005, DOI: 10.1177/1094342005056115.

[17] J. Liao *et al.*, "Toward a general I/O arbitration framework for netCDF based big data processing," in *Proc. 22nd Int. Eur. Conf. Parallel Distrib. Comput.*, Grenoble, France, pp. 293–305, 2016, DOI: 10.1007/978-3-319-43659-3_22.

[18] Meteo-France, Algorithm Theoretical Basis Document for "Cloud Products" (CMa-PGE01 v3.2, CT-PGE02 v2.2 & CTTH-PGE03 v2.2), 2013. [Online]. Available: http://www.nwcsaf.org/indexScientificDocumentation.html

[19] T. Miyoshi and K. Aranami, "Applying a four-dimensional local ensemble transform Kalman filter (4D-LETKF) to the JMA nonhydrostatic model (NHM)," *SOLA*, vol. 2, pp. 128–131, 2006, DOI: 10.2151/sola.2006-033.

[20] T. Miyoshi, Y. Sato, and T. Kadowaki, "Ensemble Kalman filter and 4D-Var intercomparison with the Japanese operational global analysis and prediction system," *Monthly Weather Rev.*, vol. 138, pp. 2846–2866, 2010, DOI: 10.1175/2010MWR3209.1.

[21] T. Miyoshi, K. Kondo, and T. Imamura, "The 10,240-member ensemble Kalman filtering with an intermediate AGCM," *Geophys. Res. Lett.*, vol. 41, 2014, DOI: 10.1002/2014GL060863.

[22] T. Miyoshi, K. Kondo, and K. Terasaki, "Big ensemble data assimilation in numerical weather prediction," *Computer*, vol. 48, pp. 15–21, 2015, DOI: 10.1109/MC.2015.332.

[23] T. Miyoshi *et al.*, ""Big Data Assimilation" revolutionizing severe weather prediction," *Bull. Amer. Meteorol. Soc.*, vol. 97, pp. 1347–1354, 2016, DOI: 10.1175/BAMS-D-15-00144.1.

[24] K. T. Murata *et al.*, "A science cloud for data intensive sciences," *Data Sci. J.*, vol. 12, pp. WDS139–WDS146, 2013, DOI: 10.2481/dsj.WDS-024.

[25] S. Nishizawa, H. Yashiro, Y. Sato, Y. Miyamoto, and H. Tomita, "Influence of grid aspect ratio on planetary boundary layer turbulence in large-eddy simulations," *Geosci. Model Dev.*, vol. 8, pp. 3393–3419, 2015, DOI: 10.5194/gmd-8-3393-2015.

[26] K. Okamoto, "Assimilation of overcast cloudy infrared radiances of the geostationary MTSAT-1R imager," *Q. J. R. Meteorol. Soc.*, vol. 139, pp. 715–730, 2013, DOI: 10.1002/qj.1994.

[27] K. Okamoto, A. P. McNally, and W. Bell, "Progress towards the assimilation of all-sky infrared radiances: An evaluation of cloud effects," *Q. J. R. Meteorol. Soc.*, vol. 140, pp. 1603–1614, 2014, DOI: 10.1002/qj.2242.

[28] A. Okuyama *et al.*, "Preliminary validation of Himawari-8/AHI navigation and calibration," J. J. Butler, X. (Jack) Xiong, and X. Gu, Eds., *SPIE—Int. Soc. Opt. Eng., Earth Observing Systems XX*, vol. 9607, 2016, 96072E, [Online]. Available: http://proceedings.spiedigitallibrary.org/proceeding.aspx?.DOI=10.1117/12.2188978

[29] M. Otsuka *et al.*, "Assimilation experiments of MTSAT rapid scan atmospheric motion vectors on a heavy rainfall event," *J. Meteorol. Soc. Jpn. Ser. II*, vol. 93, pp. 459–475, 2015, DOI: 10.2151/jmsj.2015-030.

[30] S. Otsuka *et al.*, "Precipitation nowcasting with three-dimensional space-time extrapolation of dense and frequent phased-array weather radar observations," *Weather Forecast.*, vol. 31, pp. 329–340, 2016, DOI: 10.1175/WAF-D-15-0063.1.

[31] M. Pavolonis, "Cloud Type and Cloud Phase Algorithm Theoretical Basis Document," NOAA NESDIS STAR, 2010. [Online]. Available: http://www.star.nesdis.noaa.gov/goesr/docs_reports_ATBD.php

[32] J. Ruiz, M. Pulido, and T. Miyoshi, "Estimating model parameters with ensemble-based data assimilation: A review," *J. Meteor. Soc. Jpn.*, vol. 91, pp. 79–99, 2013, DOI: 10.2151/jmsj.2013-201.

[33] J. J. Ruiz, T. Miyoshi, S. Satoh, and T. Ushio, "A quality control algorithm for the Osaka Phased Array Weather Radar," *SOLA*, vol. 11, pp. 48–52, 2015, DOI: 10.2151/sola.2015-011.

[34] K. Saito *et al.*, "The operational JMA nonhydrostatic mesoscale model," *Monthly Weather Rev.*, vol. 134, pp. 1266–1298, 2006, DOI: 10.1175/MWR3120.1.

[35] Y. Sato, S. Nishizawa, H. Yashiro, Y. Miyamoto, and H. Tomita, "Potential of retrieving shallow-cloud life cycle from future generation satellite observations through cloud evolution diagrams: A suggestion from a large eddy simulation," *SOLA*, vol. 10, pp. 10–14, 2014, DOI: 10.2151/sola.2014-003.

[36] Y. Sato *et al.*, "Horizontal distance of each cumulus and cloud broadening distance determine cloud cover," *SOLA*, vol. 11, pp. 75–79, 2015, DOI: 10.2151/sola.2015-019.

[37] Y. Sato *et al.*, "Impacts of cloud microphysics on trade wind cumulus: Which cloud microphysics processes contribute to the diversity in a large eddy simulation?," *Progr. Earth Planet. Sci.*, vol. 2, p. 23, 2015, DOI: 10.1186/s40645-015-0053-6.

[38] C. Snyder and F. Zhang, "Assimilation of simulated Doppler radar observations with an ensemble Kalman filter," *Monthly Weather Rev.*, vol. 131, pp. 1663–1677, 2003, DOI: 10.1175//2555.1.

[39] D. J. Stensrud *et al.*, "Convective-scale warn-on-forecast system: A vision for 2020," *Bull. Amer. Meteorol. Soc.*, vol. 90, pp. 1487–1499, 2009, DOI: 10.1175/2009BAMS2795.1.

[40] D. J. Stensrud *et al.*, "Progress and challenges with warn-on-forecast," *Atmos. Res.*, vol. 123, pp. 2–16, 2013, DOI: 10.1016/j.atmosres.2012.04.004.

[41] J. Sun *et al.*, "Use of NWP for nowcasting convective precipitation: Recent progress and challenges," *Bull. Amer. Meteorol. Soc.*, vol. 95, pp. 409–426, 2014, DOI: 10.1175/BAMS-D-11-00263.1.

[42] T. Ushio, T. Wu, and S. Yoshida, "Review of recent progress in lightning and thunderstorm detection techniques in Asia," *Atmos. Res.*, vol. 154, pp. 89–102, 2015, DOI: 10.1016/j.atmosres.2014.10.001.

[43] J. Wurman, P. Robinson, W. Lee, C. R. Alexander, and K. A. Kosiba, "Rapid-scan mobile radar 3D GBVTD and traditional analysis of tornadogenesis," in *Proc. 24th Conf. Severe Local Storms*, Savannah, GA, USA, 2008, p. 13.6. [Online]. Available: https://ams.confex.com/ams/24SLS/techprogram/paper_142176.htm

[44] E. Yoshikawa *et al.*, "MMSE beam forming on fast-scanning phased array weather radar," *IEEE Trans. Geosci. Remote Sens.*, vol. 51, pp. 3077–3088, 2013, DOI: 10.1109/TGRS.2012.2211607.

[45] N. Yussouf, E. R. Mansell, L. J. Wicker, D. M. Wheatley, and D. J. Stensrud, "The ensemble Kalman filter analyses and forecasts of the 8 May 2003 Oklahoma City tornadic supercell storm using single- and double-Moment microphysics schemes," *Monthly Weather Rev.*, vol. 141, pp. 3388–3412, 2013, DOI: 10.1175/MWR-D-12-00237.1.

[46] F. Zhang, Y. Weng, J. A. Sippel, Z. Meng, and C. H. Bishop, "Cloud-resolving hurricane initialization and prediction through assimilation of Doppler radar observations with an ensemble Kalman filter," *Monthly Weather Rev.*, vol. 137, pp. 2105–2125, 2009, DOI: 10.1175/2009MWR2645.1.

ABOUT THE AUTHORS

Takemasa Miyoshi received the Ph.D. degree in meteorology from the University of Maryland, College Park, MD, USA.

He leads the Data Assimilation Research Team at the RIKEN Advanced Institute for Computational Science, Kobe, Japan; is a Visiting Professor in the Department of Atmospheric and Oceanic Science, University of Maryland; and is a Visiting Senior Scientist in the Application Laboratory, Japan Agency for Marine-Earth Science and Technology, Yokohama, Japan. His research interests include numerical weather prediction, data assimilation theory, and applications.

Dr. Miyoshi is a member of the American Meteorological Society, the American Geophysical Union, the Meteorological Society of Japan, and the Japan Geoscience Union.

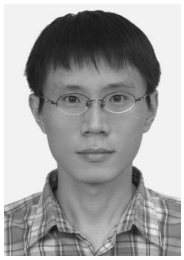

Guo-Yuan Lien received the Ph.D. degree in atmospheric science from the University of Maryland, College Park, MD, USA.

He is a Postdoctoral Researcher at the RIKEN Advanced Institute for Computational Science, Kobe, Japan. His research interests include data assimilation and tropical cyclones.

Shinsuke Satoh received the Doctor of Science degree from Hokkaido University, Hokkaido, Japan.

He is a Research Manager at the National Institute of Information and Communications Technology, Koganei, Japan. His research interests include space-borne precipitation radar, bistatic Doppler radar network, radar data application, and radar meteorology.

Dr. Satoh is a member of the American Meteorological Society, the Meteorological Society of Japan, the Visualization Society of Japan, and the Japan Geoscience Union.

Tomoo Ushio received the B.S., M.S., and Ph.D. degrees in electrical engineering from Osaka University, Osaka, Japan, in 1993, 1995, and 1998, respectively.

He was with the Global Hydrology and Climate Center, Huntsville, AL, USA, as a Postdoctorate Researcher from 1998 to 2000. In 2000, he joined the Department of Aerospace Engineering, Osaka Prefecture University, Osaka, Japan. After being an Assistant Professor at Osaka Prefecture University, in 2006, he joined the Department of Electrical, Electronic and Information Engineering, Osaka University Japan, where he is currently an Associate Professor. His research specialties are radar-based remote sensing, passive and active remote sensing of atmosphere from space-borne platforms, and atmospheric electricity.

Kotaro Bessho is a forecaster of the Tokyo Typhoon Center, Japan Meteorological Agency, Tokyo, Japan. He was a head of the System Engineering Division, Meteorological Satellite Center, Kiyose, Japan, until March 2016. His research interest is typhoon and satellite meteorology.

Dr. Bessho is a member of the American Meteorological Society and the Meteorological Society of Japan.

Hirofumi Tomita received the Dr.Eng. degree from the University of Tokyo, Tokyo, Japan.

He leads the Computational Climate Science Research Team at the RIKEN Advanced Institute for Computational Sciences, Kobe Japan. He is also the deputy project leader for Japanese flagship supercomputer project in Japan. His interest is climate modeling both in global and regional scale for high-performance computing.

Dr. Tomita is a member of the Meteorological Society of Japan and the Japan Society of Fluid Dynamics.

Seiya Nishizawa received the Ph.D. degree in science from Kyoto University, Kyoto, Japan.

He is a Research Scientist at the RIKEN Advanced Institute for Computational Science, Kobe, Japan. His research interests include atmospheric dynamics and numerical modeling.

Dr. Nishizawa is a member of the Meteorological Society of Japan and the Japanese Society for Planetary Sciences.

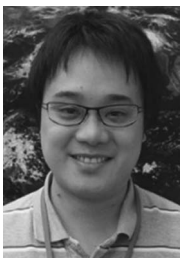

Ryuji Yoshida received the Ph.D. degree in science from Kyoto University, Kyoto, Japan.

He is a Postdoctoral Researcher at the RIKEN Advanced Institute for Computational Science, Kobe, Japan. His research interests include numerical modeling for weather and climate, high-performance computing, and mesoscale meteorology.

Dr. Yoshida is a member of the American Meteorological Society, the American Geophysical Union, and the Meteorological Society of Japan.

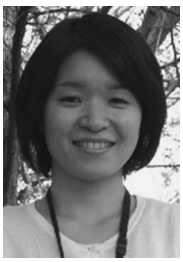

Sachiho A. Adachi received the Ph.D. degree in science from University of Tsukuba, Tsukuba, Japan.

She is a Research Scientist at the RIKEN Advanced Institute for Computational Science, Kobe, Japan. Her research interests include regional climate, atmospheric environment, and their interaction with society.

Dr. Adachi is a member of the Meteorological Society of Japan and the American Geophysical Union.

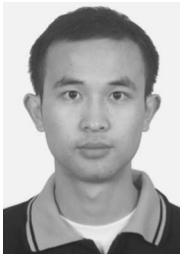

Jianwei Liao received the Ph.D. degree in computer science from the University of Tokyo, Tokyo, Japan, in 2012.

He is working for the College of Computer and Information Science, Southwest University of China, Chongqing, China. His research interests are dependable operating systems and high-performance storage systems for distributed computing environments.

Balazs Gerofi received the M.Sc. degree in computer science from the Vrije Universiteit Amsterdam, Amsterdam, The Netherlands and the Ph.D. degree in computer science from The University of Tokyo, Tokyo, Japan.

He is a Research Scientist at the RIKEN Advanced Institute for Computational Science, Kobe, Japan, where he is primarily involved with system software development for high-performance computing. His research is mainly focused on operating systems, high-performance computing, cloud computing, and fault-tolerant computing.

Dr. Gerofi is a member of the IEEE Computer Society and the Association for Computing Machinery (ACM).

Yutaka Ishikawa received the B.S., M.S., and Ph.D. degrees in electrical engineering from Keio University, Tokyo, Japan.

He is the Project Leader of the FLAGSHIP 2020 project at the RIKEN Advanced Institute for Computational Science, Kobe, Japan. From 1987 to 2001, he was a member of AIST (formerly Electrotechnical Laboratory), METI. From 1993 to 2001, he was the Chief of Parallel and Distributed System Software Laboratory, Real World Computing Partnership. From 2002 to 2006 and from 2006 to 2014, he was an Associate Professor and a Professor at the University Tokyo, Tokyo, Japan, respectively. His research interests include system software for next-generation supercomputers.

Masaru Kunii received the B.S. degree in science from the Meteorological College.

He is a Researcher at the Meteorological Research Institute, Japan Meteorological Agency, Tsukuba, Japan. His research interests include data assimilation, ensemble forecasting, and tropical cyclones.

Dr. Kunii is a member of the Meteorological Society of Japan.

Juan Ruiz received the Ph.D. degree in meteorology from the University of Buenos Aires, Buenos Aires, Brazil.

He is a Researcher at CIMA-CONICET-University of Buenos Aires and a Visiting Researcher at the RIKEN Advanced Institute for Computational Science, Kobe, Japan. His research interests include data assimilation, numerical weather prediction, and short-range forecasting.

Yasumitsu Maejima received the M.S. degree in science from Kyushu University, Fukuoka, Japan.

He is a Research Associate at the RIKEN Advanced Institute for Computational Science, Kobe, Japan. His research interests include data assimilation, mesoscale meteorology, and local heavy rainfall prediction.

Mr. Maejima is a member of the Meteorological Society of Japan and the Japan Geoscience Union.

Shigenori Otsuka received the Ph.D. degree in science from Kyoto University, Kyoto, Japan.

He is a Research Scientist at the RIKEN Advanced Institute for Computational Science, Kobe, Japan. His research interests include meteorology and data assimilation.

Dr. Otsuka is a member of the Meteorological Society of Japan and the Japan Geoscience Union.

Michiko Otsuka received the M.S. degree from the Tokyo Metropolitan University, Tokyo, Japan.

She is a Senior Researcher at the Meteorological Research Institute of the Japan Meteorological Agency, Tsukuba, Japan. Her research interest includes data assimilation, numerical weather prediction, and meteorological observation.

Miss Otsuka is a member of the Meteorological Society of Japan.

Kozo Okamoto received the Ph.D. degree in science from the University of Tohoku, Sendai, Japan.

He is a Senior Researcher of the Meteorological Research Institute of Japan Meteorological Agency, Tsukuba, Japan. His research interests include satellite data assimilation and typhoon analysis.

Dr. Okamoto is a member of the Meteorological Society of Japan.

Hiromu Seko received the Ph.D. degree in science from Tokyo University, Tokyo, Japan.

He is the Head of the 2nd Laboratory of Forecast Research Department, Meteorological Research Institute, Tsukuba, Japan. His research interests include data assimilation, ensemble forecast, numerical weather prediction, and high-performance computing.

Dr. Seko is a member of the Meteorological Society of Japan and the American Meteorological Society.